Advances in Bioresearch
Adv. Biores., Vol 14 (6) November 2023: 320-341
©2023 Society of Education, India
Print ISSN 0976-4585; Online ISSN 2277-1573
Journal's URL:http://www.soeagra.com/abr.html
CODEN: ABRDC3
DOI: 10.15515/abr.0976-4585.14.6.320341

Advances in Bioresearch

ORIGINAL ARTICLE

In Silico driven synthesis and Biological Evaluation of some ethyl 2-(((1*H*-benzo[*d*]imidazol-2-yl)methyl) amino) thiazole-4-carboxylate derivatives as VEGFR-2 inhibitors

Ashwini B. Patil1*, Kamalkishor G. Baheti[1]
[1]Y. B. Chavan College of Pharmacy, Aurangabad, Maharashtra 431003, India
***Corresponding author email: ashwinipatil2020@yahoo.com**

ABSTRACT
In current study, we have designed and developed some ethyl 2-(((1H-benzo[d]imidazol-2-yl)methyl)amino)thiazole-4-carboxylate derivatives as potential VEGFR-2 kinase inhibitors for the treatment of cancer. Out of the 30 screened derivatives (AP31-AP60), AP35, AP37, AP41, AP42, AP47, AP48, AP50, AP51, AP55, and AP58 exhibited binding affinity greater than native ligand and formed four and more than four hydrogen bonds with enzyme are considered as most potent and hence selected for wet lab synthesis. The compounds AP47 and AP50 showed excellent VEGFR2 kinase inhibitory activity at IC_{50} 2.77 and 4.90 µM respectively whereas pazopanib displayed VEGFR2 kinase inhibitory activity at 0.092 µM. Compound AP47 was found to be the most potent VEGFR2 inhibitor. Among the tested compounds, it has been noticed that compound AP47 was found to be the most potent compound against A-549, HEK-293, and MCF-7 with GI_{50} values of 6.13, 8.24, and 9.36 µM, respectively. Only this compound showed moderate cytotoxicity against MDA-MB-231(GI_{50} =23.65 µM). Compound AP48 showed good anti-cancer activity against A-549 at GI_{50} values of 8.07 µM, respectively. Compounds (AP41, AP50, AP55, and AP58) showed moderate potency against A-549, MCF-7 and HEK-293 (<25 µM). SAR studies of the synthesized benzo-imidazole compounds revealed the anti-cancer activity dependent on the type of substitutions present on the cyclohexadiene ring attached to the benzo-imidazole ring. The presence of thiazole-4-carboxylate linked through methyl amino to benzo-imidazole ring showed improved activity against A-549, HEK-293, and MCF-7 cancer cell lines. The results from the current study indicate that these compounds have promising future use as VEGFR2 kinase inhibitors.

Keywords: *VEGFR-2 kinase; inhibitors; cancer; rational drug design; synthesis; in vitro*

Received 29.08.2023 Revised 18.09.2023 Accepted 23.10.2023

How to cite this article:
Ashwini B. Patil, Kamalkishor G. Baheti. *In Silico* driven synthesis and Biological Evaluation of some ethyl 2-(((1*H*-benzo[*d*]imidazol-2-yl)methyl) amino) thiazole-4-carboxylate derivatives as VEGFR-2 inhibitors. Adv. Biores., Vol 12 (6) November 2023: 320-341.

INTRODUCTION

VEGFR-2 is an acronym for Vascular Endothelial Growth Factor Receptor 2, a protein that has a crucial function in the creation of blood vessels, also known as angiogenesis. A receptor tyrosine kinase is a protein located on the cell surface that has the ability to bind to certain signaling chemicals called growth factors[1]. VEGFR-2 interacts with vascular endothelial growth factors (VEGFs), which are proteins that promote angiogenesis. Comprehending the role and control of VEGFR-2 is crucial in both normal body processes and abnormal circumstances, especially in the field of cancer investigation and the development of specific treatments. Scientists and healthcare professionals are still studying methods to control the VEGF/VEGFR-2 pathway for purposes of treatment in cancer[2,3]. There are many VEGFR-2 kinase inhibitors in the market as depicted in Figure 1.

VEGFR-2 kinase inhibitors are a notable breakthrough in cancer therapy since they specifically target the crucial mechanism of angiogenesis. Their capacity to hinder the development of new blood vessels in tumours has shown efficacy in reducing tumour growth, inhibiting metastasis, and enhancing overall patient outcomes in certain cancer types. These inhibitors remain crucial in targeted cancer therapy, either as independent treatments or in conjunction with other therapeutic methods[4–8]. In current

study, we have designed and developed some ethyl 2-(((1*H*-benzo[*d*]imidazol-2-yl)methyl)amino)thiazole-4-carboxylate derivatives as potential VEGFR-2 kinase inhibitors for the treatment of cancer.

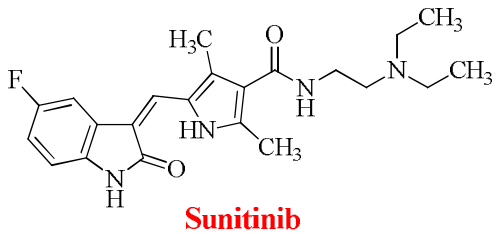

Sunitinib

It has received approval for the treatment of many types of malignancies, including as renal cell carcinoma and gastrointestinal stromal tumours.

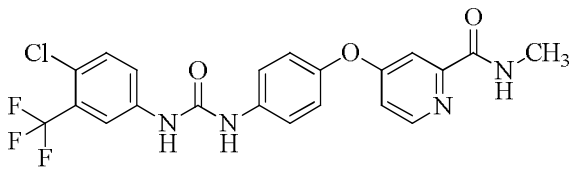

Sorafenib

It is used for the treatment of advanced renal cell carcinoma, hepatocellular carcinoma, and thyroid cancer.

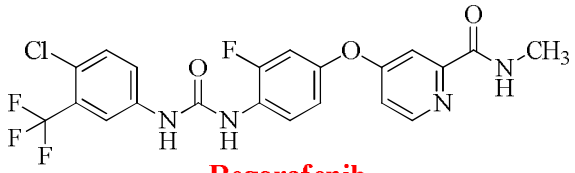

Regorafenib

This medication is used for the treatment of colorectal cancer, gastrointestinal stromal tumours, and hepatocellular carcinoma.

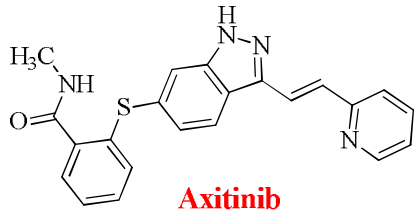

Axitinib

It is specifically inhibits the activity of VEGFR-1, VEGFR-2, and VEGFR-3. It has received approval for treating advanced renal cell cancer after unsuccessful earlier systemic therapy.

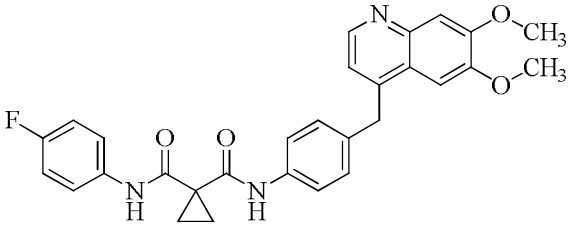

Cabozantinib

It has received approval for the treatment of medullary thyroid cancer and advanced renal cell carcinoma.

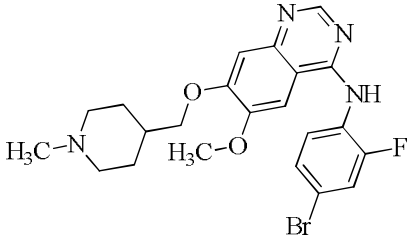

Vandetanib

It has received approval for the therapeutic use in cases of medullary thyroid carcinoma.

Figure 1. The approved VEGFR-2 kinase inhibitors

MATERIAL AND METHODS

Pre-ADMET Analysis

Mol Inspiration, a free service for the online chemistry community, provides access to molecular metrics like logP, polar surface area, number of hydrogen bond donors and acceptors (GPCR ligands, kinase inhibitors, ion channel modulators, nuclear receptors), and bioactivity score prediction for the most significant drug targets. The SwissADME online tool may be used to compute physicochemical descriptors and predict ADME parameters, pharmacokinetic properties, drug-like nature, and medicinal chemistry friendliness of one or more small molecules to assist in drug development. Utilizing mol inspiration (https://www.molinspiration.com/) and Swiss ADME servers (http://www.swissadme.ch/), Lipinski rule of five and pharmacokinetic features of designed derivatives were investigated[9–12].

Toxicity prediction is an important phase in the development of novel medications. The use of computational toxicity estimations as opposed to animal toxic dose assessments may reduce the number of animal investigations. Toxicological endpoints, including acute toxicity, liver toxicity, cell death, carcinogenicity, mutation, immunotoxicity, unfavorable outcomes (Tox21) pathways, and toxicity targets are all covered in ProTox-arsenal II's of 33 different toxicity endpoint prediction models. This incorporates (fragment similarity-based CLUSTER cross-validation) machine learning as well as molecular similarity and fragment propensity. Utilising the freely available web server ProTox-II, an in silico assessment of the toxicity potential of designed derivatives was conducted (http://tox.charite.de/protox_II)[13].

Screening through Molecular Docking

Molecular docking is a fundamental aspect of computer-assisted drug discovery and structural molecular biology. Using a method known as "ligand-protein docking," scientists may foretell how a ligand will interact with a protein whose three-dimensional structure is already known. A precise scoring system for dockings in high-dimensional areas is essential. One may do virtual screening on a large library of compounds, grade the results, and propose structural ideas of how the ligands block the target, which is highly valuable in lead optimization[14–18].

Following an initial screening process utilizing *In Silico* ADMET analysis, the selected molecules underwent subsequent molecular docking studies. In order to achieve further optimization, the derivatives underwent binding affinity studies with the target enzyme. All the selected compounds and the native ligand were docked against the Crystal structure of the KDR (VEGFR2) kinase domain in complex with a type-II inhibitor bearing an acrylamide using Autodock vina 1.1.2 in PyRx 0.8[19]. ChemDraw Ultra 8.0 was used to draw the structures of the compounds and native ligand (mole. File format). All the ligands were subjected for energy minimization by applying Universal Force Field (UFF)[20]. The crystal structure of the enzyme with PDB ID: 6XVK was obtained from RCSB Protein Data Bank (PDB) (https://www.rcsb.org/structure/6XVK). Discovery Studio Visualizer (version-19.1.0.18287) was used to refine the enzyme structure, purify it, and get it ready for docking[21]. A three-dimensional grid box with an exhaustiveness value of 8 was created for molecular docking[19]. BIOVIA Discovery Studio Visualizer was used to locate the protein's active amino acid residues. The approach outlined by Khan et al. was used to perform the entire molecular docking procedure, identify cavity and active amino acid residues[22–28]. Figure 2 shows the revealed cavity of enzyme with the native ligand.

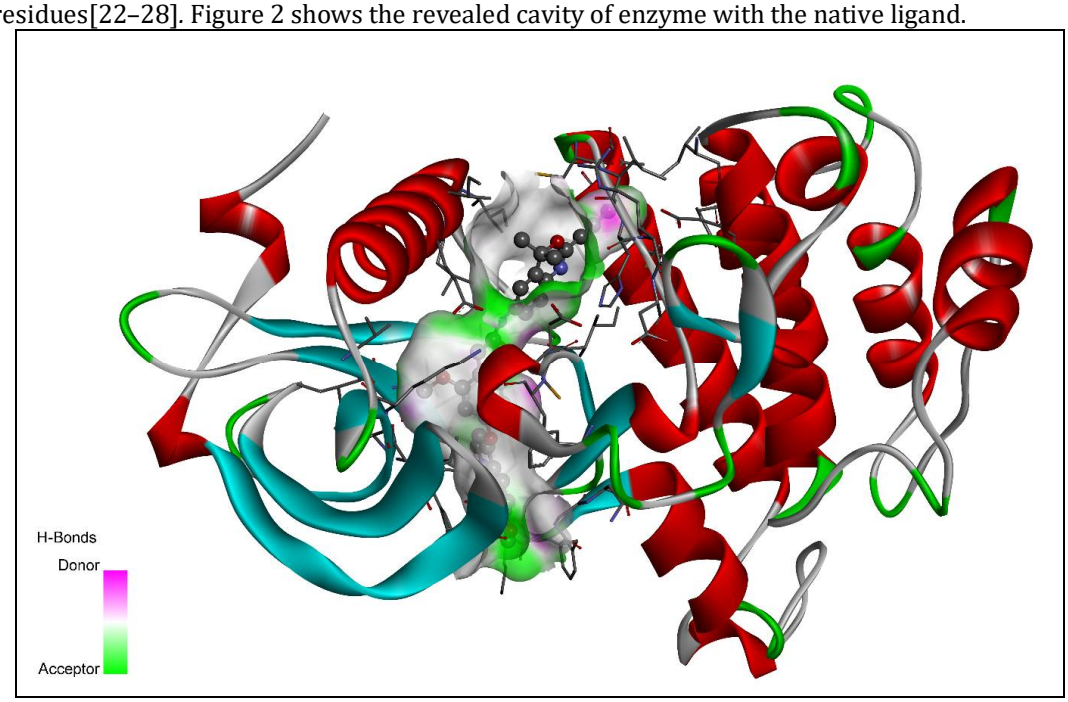

Figure 2. The 3D ribbon view of the enzyme with native ligand in the cavity

Chemistry

Chemicals, Reagents, and Cell Lines

From Lab Trading Laboratory in Aurangabad, Maharashtra, India, all of the essential chemicals and reagents of synthetic quality were obtained and procured. Through the use of thin-layer chromatography (TLC, Merck precoated silica GF 254), the progression of the reaction was seen and verified. Spectral analysis was performed on the compounds using ^{1}H NMR, ^{13}C NMR (on a Varian-VXR-300S @ 400 MHz NMR spectrometer), and Mass spectroscopy. Chloroform (d_6) was used as the solvent, and TMS was used as the internal standard. Chemical shift values were stated in δ ppm. The melting points were determined with the assistance of a melting point equipment of VEEGO MODEL VMP-D.

All the cell lines: MCF-7 (estrogen dependent) & MDA-MB-231(non-estrogen dependent) human breast adenocarcinoma epithelial cell lines, HEK-293 (human kidney carcinoma cell line), A549 (lung adenocarcinoma cell line), NIH/3T3 (embryonic mouse fibroblast cell line) were purchased from National Centre for Cell Science (NCCS), Pune, India. On receipt, the cell lines were passaged in our lab and the earliest passaged cells were cryopreserved in liquid nitrogen container for future use. The cell lines used

in culture were passaged for fewer than 8 weeks and were carefully maintained as described. The cells were maintained in Dulbecco's modified Eagle medium (DMEM) (Cell clone genetix brand, Catalogue No.: CC3004) complete media with 10% fetal bovine serum (Cell clone genetix brand, Catalogue No.: CCS-500-SA-U3034)) and penicillin–streptomycin (50 U/ml, 50 mg/ml; HiMedia, Catalogue No.: A002) at 37°C, CO2 (5%) and air (95%). Around 70–80% confluency of cultured cells was used for seeding during the assays. Dulbecco's phosphate-buffered saline (Cell clone genetix brand, Catalogue No.: CC3034), trypan blue (Bio-Rad, catalogue no: 1450013).

Synthesis

Step-I: Synthesis of 2-(chloromethyl)-1H-benzo[d]imidazole

O-Phenylenediamine (OPD) (1.08 gm, 0.01 mol.), chloroacetyl chloride (1.12 gm, 0.01 mol.) and 4N hydrochloric acid (100 cc.) were refluxed at 60-70 ^{0}C for about 3-4 hours. The mixture was allowed to stand overnight, filtered, diluted with 200 cc. of water, cooled and carefully neutralized with 6N sodium hydroxide (NaOH) solution. The solution was kept cold during the neutralization and stirred vigorously to prevent the formation of gums. After neutralization, the solution was stirred vigorously until the formation of light brown precipitate. The product was filtered, washed well with cold water. It was then placed in a vacuum desiccator until dry. The yields obtained were 87%. The product was obtained as yellowish-brown by recrystallization from dioxane; m.p. 150-152 ^{0}C (Lit. 147.8–148.2 ^{0}C). Care was taken while handling 2-(chloromethyl)-1*H*-benzimidazole since it is a powerful skin and mucous membrane irritant. The completion of the reaction was monitored by thin-layer chromatography (TLC) using Benzene: Methanol (8:2) solvent system. After visualization in the iodine chamber, the run of reaction mixture did not show the spot in front of the reactant (OPD) which indicates the completion of the reaction and the spot of the product was clearly observed[28].

Step-II: Synthesis of ethyl 2-(((1H-benzo[d]imidazol-2-yl)methyl)amino)thiazole-4-carboxylate

A mixture of 2-(chloromethyl)-1*H*-benzo[*d*]imidazole (3mmol), ethyl 2-aminothiazole-4-carboxylate (3mmol), and K_2CO_3 (3mmol) in 20 mL ethanol and 5 mL DMF was refluxed at 60-70 ^{0}C for about 8-10 hours. Completion of the reaction was monitored by TLC (Ethyl acetate:benzene:ethanol; 4:4:2). After the reaction completion, the excess solvent was evaporated under reduced pressure, poured onto ice and the pH was adjusted to pH (6-8). The formed solid was collected by vacuum filtration. The obtained products have been studied for physical characterization and recrystallized using ethanol[29]. The % yield of the product was 79%.

Step-III: Synthesis of ethyl 2-(((1H-benzo[d]imidazol-2-yl)methyl)amino)thiazole-4-carboxylate derivatives

Out of the 30 screened derivatives (AP31-AP60), **AP35, AP37, AP41, AP42, AP47, AP48, AP50, AP51, AP55,** and **AP58** exhibited binding affinity greater than native ligand and formed four and more than four hydrogen bonds with enzyme are considered as most potent and hence selected for wet lab synthesis.

Ethyl 2-(((1*H*-benzo[*d*]imidazol-2-yl)methyl)amino)thiazole-4-carboxylate (1 mmol) and appropriate aldehydes (1 mmol) in glacial acetic acid (10 mL) and ethanol (10 mL) were refluxed for 1-1.5 hrs. The reaction mixture was then cooled and poured into ice-cold water and solid was filtered out. The dried solid was recrystallized from ethanol to give ethyl 2-(((1*H*-benzo[*d*]imidazol-2-yl)methyl)amino)thiazole-4-carboxylate derivatives. The completion of reaction was monitored using TLC using Ethyl acetate:benzene:ethanol (4:4:2) as solvent system[30,31]. The % yield of the products were between 45-65%. The structures of the obtained products were then confirmed by FTIR, Mass, ^{1}H NMR, and ^{13}C NMRs. The proposed reaction scheme is depicted in Figure 3. The different substitutions used for designing of derivatives AP31 to AP60 are tabulated in Table 1.

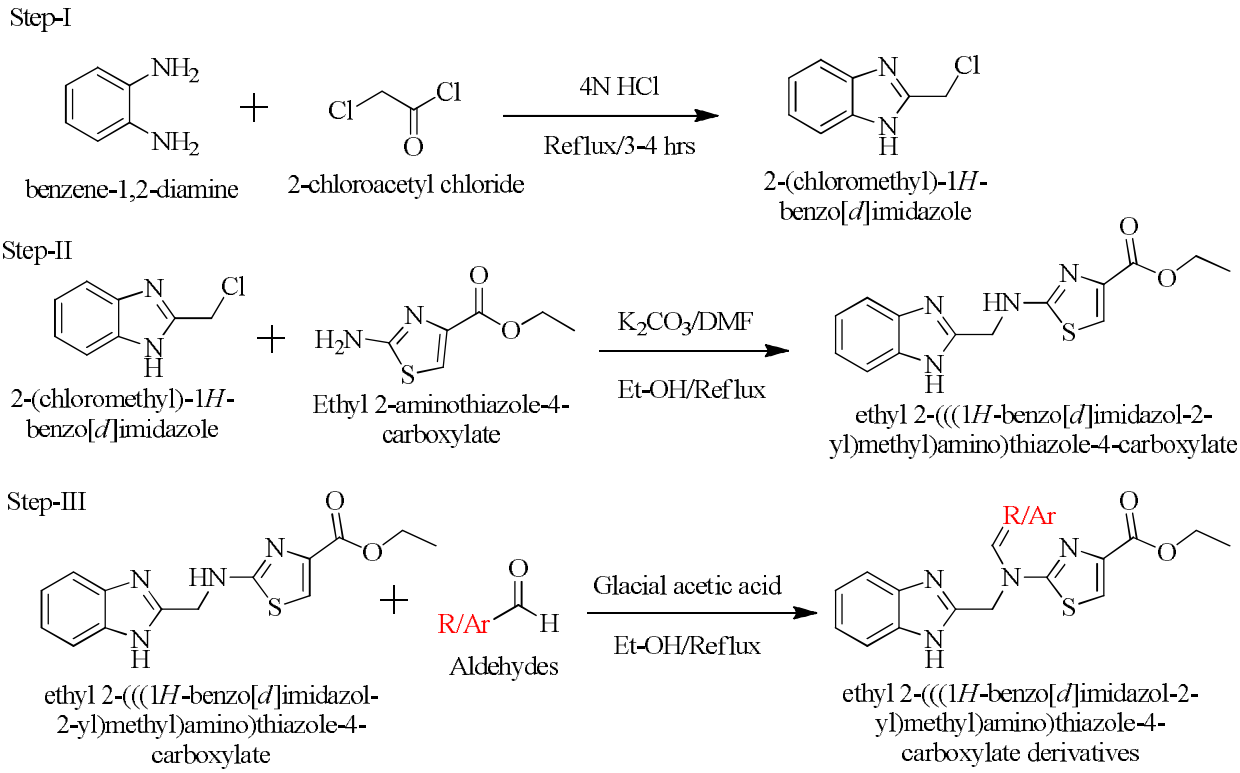

Figure 3. The proposed reaction scheme for the synthesis of ethyl 2-(((1*H*-benzo[*d*]imidazol-2-yl)methyl)amino)thiazole-4-carboxylate derivatives

Spectral analysis of synthesized compounds

Step-I: 2-(chloromethyl)-1H-benzo[d]imidazole

Mol. Wt: 166.61, Rf value: 0.92, Melting point (^{0}C): 150-152, Appearance: Yellowish brown solid, % yield: 59. FT-IR (neat, cm -1) νmax: 3697.39 (NH- stretch), 3609.39 (-CH stretch), 2806.39 (-CH bend), 1891.49 (-C=N stretch), 1866.37 (-C=C stretch), 1110.04 (-CN stretch), 781.39 (C-Cl). ^{1}H NMR (300 MHz, Chloroform (d_6), chemical shift (ppm)); δ 5.17 (d, NH of imidazole), 7.16, 7.17, 7.18, 7.19, 7.20, 7.21, 7.22, 7.44, 7.45, 7.46, 7.47, 7.48, 7.56, 7.57, 7.58. (s, Ar- CH). ^{13}C NMR (300 MHz, Chloroform (d_6), chemical shift (ppm)); δ 14.82, 37.50, 116.54, 123.29, 124.07, 126.63, 135.70, 138.75, 154.23. MS: 168.28.

Step-II: Ethyl 2-(((1H-benzo[d]imidazol-2-yl)methyl)amino)thiazole-4-carboxylate

Mol. Wt: 302.35, Rf value: 0.47, Melting point (^{0}C): 168-170, Appearance: yellowish orange solid, % yield: 79. FT-IR (neat, cm -1) νmax: 3559.18 (NH- stretch), 3419.57 (-CH stretch), 3118.47 (-CH bend), 1949.30 (-C=N stretch), 1578.27 (-C=C stretch), 1136.20 (-CN stretch), 898.78 (-Cl). ^{1}H NMR (300 MHz, Chloroform (d_6), chemical shift (ppm)); δ 4.39 (d, NH of imidazole), 7.23, 7.24, 7.26, 7.30, 7.34, 7.35, 7.36, 7.43, 7.44, 7.45 (s, Ar- CH), 8.94, 8.96 (d, NH of thiazole), 9.47 (s, NH). ^{13} C NMR (300 MHz, Chloroform (d_6), chemical shift (ppm)); δ 18.47, 21.71, 43.03, 95.07, 112.46, 121.16, 123.76, 124.16, 129.48, 135.59, 137.18, 143.52, 152.74, 161.64, 168.12. MS: 305.29.

AP35: (E)-ethyl 2-(((1H-benzo[d]imidazol-2-yl)methyl)((4-fluorocyclohexa-2,4-dien-1-ylidene) methyl) amino) thiazole-4-carboxylate

Mol. Wt: 410.46, Rf value: 0.78, Melting point (^{0}C): 177-179, Appearance: light brown solid, % yield: 61. FT-IR (neat, cm -1) νmax: 3681.14 (NH- stretch), 3626.78 (-CH stretch), 3010.21 (-CH bend), 1949.67 (-C=N stretch), 1668.39 (-C=C stretch), 1438.45 (-CN stretch), 918.30 (-Cl). ^{1}H NMR (300 MHz, Chloroform (d_6), chemical shift (ppm)); δ 1.35, 1.36, 1.37 (-COOH), 4.39, 4.40, 4.41, 4.43 (d, NH of imidazole), 5.35, 6.02, 6.04, 6.05, 6.35, 6.39, 6.80, 6.81 (-C_6H_5F), 7.17, 7.18, 7.19, 7.20, 7.45, 7.46, 7.47, 7.49, 7.57, 7.58 (s, Ar- CH), 8.94, 8.96 (d, NH of thiazole), 9.47 (s, NH). ^{13} C NMR (300 MHz, Chloroform (d_6), chemical shift (ppm)); δ 14.34, 20.15, 2018, 28.32, 28.42, 50.44, 61.43, 93.02, 93.18, 96.43, 111.50, 118.89, 119.75, 119.75, 119.77, 119.87, 120.05, 123.10, 132.52, 135.65, 137.11, 137.19, 141.25, 146.27, 149.69,158.29, 160.24, 160.85, 160.92. MS: 411.13.

AP37: (E)-ethyl 2-(((1H-benzo[d]imidazol-2-yl)methyl)((4-methylcyclohexa-2,4-dien-1-ylidene)methyl) amino)thiazole-4-carboxylate

Mol. Wt: 406.50, Rf value: 0.79, Melting point (^{0}C): 199-201, Appearance: off white solid, % yield: 54. FT-IR (neat, cm -1) νmax: 3905.29 (NH- stretch), 3343.56 (-CH stretch), 2974.58 (-CH bend), 2029.53 (-C=N

stretch), 1537.47 (-C=C stretch), 1106.17 (-CN stretch). ^{1}H NMR (300 MHz, Chloroform (d_6), chemical shift (ppm)); δ 1.35, 1.36, 1.37 (-COOH), 4.39, 4.40, 4.41, 4.43 (d, NH of imidazole), 5.63, 5.64, 5.65, 5.81, 6.68, 6.69, 6.70, 6.81, 6.68, 6.69, 6.70, 6.81, 6.82, 6.83 (-C_6H_5F), 7.23, 7.24, 7.25, 7.32, 7.33, 7.39, 7.40, 7.48, 7.84, 7.85 (s, Ar- CH). ^{13} C NMR (300 MHz, Chloroform (d_6), chemical shift (ppm)); δ 14.34, 21.36, 21.61, 30.27, 50.35, 61.43, 108.40, 113.43, 114.28, 115.88, 119.97, 123.10, 123.63, 134.26, 135.30, 136.58, 137.51, 140.90, 141.23, 149.96, 160.92, 160.99, 164.30. MS: 408.00.

AP41: (E)-ethyl 2-(((1H-benzo[d]imidazol-2-yl)methyl)((3-hydroxycyclohexa-2,4-dien-1-ylidene)methyl) amino) thiazole-4-carboxylate

Mol. Wt: 408.4, Rf value: 0.68, Melting point (^{0}C): 261-263, Appearance: yellowish brown solid, % yield: 63. FT-IR (neat, cm -1) νmax: 3651.48 (NH- stretch), 3387.37 (-CH stretch), 2934.12 (-CH bend), 2071.49 (-C=N stretch), 1572.78 (-C=C stretch), 997.48 (-CN stretch). ^{1}H NMR (300 MHz, Chloroform (d_6), chemical shift (ppm)); δ 1.35, 1.36, 1.37 (-COOH), 4.39, 4.40, 4.41, 4.43 (d, NH of imidazole), 5.63, 5.64, 5.65, 5.81, 6.68, 6.69, 6.70, 6.81, 6.68, 6.69, 6.70, 6.81, 6.82, 6.83 (-C_6H_6 O), 7.23, 7.24, 7.25, 7.32, 7.34, 7.49 (s, Ar- CH). ^{13} C NMR (300 MHz, Chloroform (d_6), chemical shift (ppm)); δ 14.34, 21.36, 21.36, 29.01, 61.43, 78.85, 106.12, 113.81, 114.35, 120.95, 122.58, 123.85, 125.43, 134.46, 135.32, 136.46, 136.49, 136.53, 140.81, 153.92, 160.25, 160.25, 160.91, 164.85. MS: 409.34.

AP42: (E)-ethyl 2-(((1H-benzo[d]imidazol-2-yl)methyl)((2,3,4-trihydroxycyclohexa-2,4-dien-1-ylidene) methyl) amino)thiazole-4-carboxylate

Mol. Wt: 440.47, Rf value: 0.71, Melting point (^{0}C): 269-271, Appearance: brownish sticky solid, % yield: 50. FT-IR (neat, cm -1) νmax: 3629.77 (NH- stretch), 3098.41 (-CH stretch), 3069.89 (-CH bend), 1949.30 (-C=N stretch), 1578.27 (-C=C stretch), 1136.20 (-CN stretch). ^{1}H NMR (300 MHz, Chloroform (d_6), chemical shift (ppm)); δ 1.35, 1.36, 1.37 (-COOH), 4.39, 4.40, 4.41, 4.43 (d, NH of imidazole), 5.35, 5.97, 5.98, 5.99, 6.97, 6.98 (-C_6H_6 O), 7.14, 7.22, 7.23, 7.24, 7.28, 7.30, 7.34, 7.49, 7.95 (s, Ar- CH). ^{13} C NMR (300 MHz, Chloroform (d_6), chemical shift (ppm)); δ 14.34, 29.89, 61.43, 72.28, 102.05, 115.22, 117.78, 122.66, 123.05, 123.19, 125.66, 136.59, 137.19, 138.17, 138.55, 14085, 148.82, 151.77, 153.89, 160.90, 161.00.. MS: 440.89.

AP47: (E)-ethyl 2-(((1H-benzo[d]imidazol-2-yl)methyl)((2,4-dinitrocyclohexa-2,4-dien-1-ylidene)methyl) amino)thiazole-4-carboxylate

Mol. Wt: 442.47, Rf value: 0.85, Melting point (^{0}C): 253-255, Appearance: brownish solid, % yield: 47. FT-IR (neat, cm -1) νmax: 3609.77 (NH- stretch), 3267.38 (-CH stretch), 3002.46 (-CH bend), 1907.56 (-C=N stretch), 1510.39 (-C=C stretch), 992.08 (-CN stretch). ^{1}H NMR (300 MHz, Chloroform (d_6), chemical shift (ppm)); δ 1.35, 1.36, 1.37 (-COOH), 3.66, 3.67, 3.68, 4.39, 4.40, 4.41, 4.43, 5.35, 6.95, 6.96 (d, NH of imidazole), 7.23, 7.24, 7.25, 7.31, 7.32, 7.36, 7.38, 7.49, 7.81, 7.82, 7.83 (-C_6H_6 O), 8.03 (s, Ar- CH). ^{13} C NMR (300 MHz, Chloroform (d_6), chemical shift (ppm)); δ 14.34, 21.36, 35.75, 61.43, 78.62, 108.42, 113.81, 114.35, 122.58, 122.99, 123.26, 123.85, 134.46, 135.59, 136.49, 136.53, 140.81, 141.38, 141.42, 153.77, 159.94, 160.91. MS: 482.78.

AP48: (E)-ethyl 2-(((1H-benzo[d]imidazol-2-yl)methyl)((4-(methylsulfonyl)cyclohexa-2,4-dien-1-ylidene) methyl)amino)thiazole-4-carboxylate

Mol. Wt: 470.56, Rf value: 0.80, Melting point (^{0}C): >280 (decomposed), Appearance: yellowish brown solid, % yield: 58. FT-IR (neat, cm -1) νmax: 3663.29 (NH- stretch), 3369.45 (-CH stretch), 2982.19 (-CH bend), 2073.49 (-C=N stretch), 1618.30 (-C=C stretch), 1052.19 (-CN stretch). ^{1}H NMR (300 MHz, Chloroform (d_6), chemical shift (ppm)); δ 1.35, 1.36, 1.37 (-COOH), 3.30, 3.31, 3.32, 3.44, 4.40, 4.41, 4.43, 5.35, 6.25, 6.73, 6.74, 6.76, 6.84, 6.85 (d, NH of imidazole), 7.16, 7.17, 7.18, 7.19, 7.20, 7.21, 7.22, 7.45, 7.47, 7.49, 7.57, 7.58 (-C_6H_6 O), 9.78 (s, Ar- CH). ^{13} C NMR (300 MHz, Chloroform (d_6), chemical shift (ppm)); δ 14.34, 21.36, 26.22, 41.28, 61.43, 78.82, 113.81, 114.35, 122.58, 123.85, 124.40, 125.37, 12.36, 131.05, 132.30, 134.46, 135.34, 136.49, 136.53, 140.81, 153.92, 160.26, 160.91. MS: 470.88.

AP50: (E)-ethyl 2-(((1H-benzo[d]imidazol-2-yl)methyl)((4-(trifluoromethyl)cyclohexa-2,4-dien-1-ylidene) methyl)amino)thiazole-4-carboxylate

Mol. Wt: 460.47, Rf value: 0.65, Melting point (^{0}C): 193-195, Appearance: pale yellow solid (Sticky), % yield: 52. FT-IR (neat, cm -1) νmax: 3769.45 (NH- stretch), 3489.44 (-CH stretch), 3084.51 (-CH bend), 2190.45(-C=N stretch), 1791.17 (-C=C stretch), 1032.29 (-CN stretch). ^{1}H NMR (300 MHz, Chloroform (d_6), chemical shift (ppm)); δ 1.35, 1.36, 1.37 (-COOH), 3.30, 3.31, 3.32, 3.44, 4.40, 4.41, 4.43, 5.35, 6.25, 6.73, 6.74, 6.76, 6.84, 6.85 (d, NH of imidazole), 7.16, 7.17, 7.18, 7.19, 7.20, 7.21, 7.22, 7.45, 7.47, 7.49, 7.57, 7.58 (-C_6H_6 O), 9.78 (s, Ar- CH).^{13} C NMR (300 MHz, Chloroform (d_6), chemical shift (ppm)); δ 14.34, 21.36, 28.65, 28.67, 28.69, 28.70, 50.35, 61.43, 101.14, 101.17, 101.19, 101.22, 104.88, 104.92, 104.95, 104.98, 113.43, 115.88, 118.04, 120.36, 122.39, 123.10, 123.63, 124.56, 131.40, 131.65, 131.89, 134.26, 135.58, 140.85, 141.23, 149.96, 160.92, 160.99, 163.63, 163.65, 163.68, 163.71. MS: 461.00.

AP51: ethyl 2-(((1H-benzo[d]imidazol-2-yl)methyl)(vinyl)amino)thiazole-4-carboxylate
Mol. Wt: 328.39, Rf value: 0.84, Melting point (^{0}C): 127-129, Appearance: pale orange solid, % yield: 46. FT-IR (neat, cm -1) νmax: 3620.18 (NH- stretch), 3239.19 (-CH stretch), 2673.19 (-CH bend), 2073.49 (-C=N stretch), 1687.30 (-C=C stretch), 1508.39 (-CN stretch). ^{1}H NMR (300 MHz, Chloroform (*d_6*), chemical shift (ppm)); δ 1.35, 1.36, 1.37 (-COOH), 3.30, 3.31, 3.32, 3.44, 4.40, 4.41, 4.43, 5.35, 6.25, 6.73, 6.74, 6.76, 6.84, 6.85 (d, NH of imidazole), 7.16, 7.17, 7.18, 7.19, 7.20, 7.21, 7.22, 7.45, 7.47, 7.49, 7.57, 7.58 (-C_6H_6 O), 9.78 (s, Ar- CH). ^{13} C NMR (300 MHz, Chloroform (*d_6*), chemical shift (ppm)); δ 14.34, 15.93, 61.43, 72.05, 90.69, 100.35, 115.08, 121.15, 122.68, 134.22, 135.56, 137.03, 140.84, 150.76, 154.76, 154.49, 160.90, 161.87. MS: 329.00.
AP55: ethyl 2-(((1H-benzo[d]imidazol-2-yl)methyl)(cyclopropylidenemethyl)amino)thiazole-4-carboxylate
Mol. Wt: 354.43, Rf value: 0.78, Melting point (^{0}C): 215-217, Appearance: blackish brown solid, % yield: 49. FT-IR (neat, cm -1) νmax: 3587.22 (NH- stretch), 3029.23(-CH stretch), 2991.16 (-CH bend), 1909.12 (-C=N stretch), 1596.20 (-C=C stretch), 1011.33 (-CN stretch). ^{1}H NMR (300 MHz, Chloroform (*d_6*), chemical shift (ppm)); δ 2.71, 4.39 (d, NH of imidazole), 5.16, 5.19, 5.39, 5.41, 5.68, 5.69, 5.70, 5.71, 5.72, 6.57, 6.59, 6.60, 6.62 (cyclopropylidenemethyl)amino), 7.24, 7.25, 7.26, 7.33, 7.35, 7.36, 7.48, 7.64, 7.65 (s, Ar- CH). ^{13} C NMR (300 MHz, Chloroform (*d_6*), chemical shift (ppm)); δ 2.53, 5.22, 14.34, 19.19, 53.99, 61.43, 96.76, 111.76, 117.49, 123.01, 125.96, 132.68, 134.14, 138.49, 140.59, 146.47, 155.26, 160.92, 162.41. MS: 353.18.
AP58: (E)-ethyl 2-(((1H-benzo[d]imidazol-2-yl)methyl)((2,6-dimethylcyclohexa-2,4-dien-1-ylidene)methyl) amino)thiazole-4-carboxylate
Mol. Wt: 420.53, Rf value: 0.83, Melting point (^{0}C): 223-225, Appearance: brown solid (Sticky), % yield: 60. FT-IR (neat, cm -1) νmax: 3794.10 (NH- stretch), 3549.89 (-CH stretch), 3129.78 (-CH bend), 1972.67 (-C=N stretch), 1578.27 (-C=C stretch), 1019.46 (-CN stretch). ^{1}H NMR (300 MHz, Chloroform (*d_6*), chemical shift (ppm)); δ 1.19, 1.20, 1.35, 1.36, 1.37, 1.78, 1.79, 1.84, 2.42, 3.03, 3.05, 3.06, 4.39, 4.40, 4.41, 4.41, 4.43 (d, NH of imidazole), 5.34, 6.18, 6.19, 6.20, 6.41, 6.43, 7.23, 7.24, 7.25, 7.28, 7.29, 7.31, 7.32,7.36, 7.38, 7.49 (d, NH of thiazole), 9.45 (s, NH). ^{13} C NMR (300 MHz, Chloroform (*d_6*), chemical shift (ppm)); δ 14.43, 21.10, 21.14, 22.09, 30.86, 50.30, 80.11, 112.00, 114.37, 116.82, 123.15, 124.94, 124.96, 127.18, 129.47, 132.15, 135.06, 135.08, 138.47, 142.08, 151.16, 153.70, 161.06, 162.46. MS: 420.06.

Biological Evaluation

VEGFR2 (KDR kinase inhibitory activity assay)

All the reagents and working standards were prepared according to the BPS Biosciences (product code: 40325, San Diego, CA, USA) to measure the VEGFR2 (KDR) kinase activity by quantification. Stock solutions of Pazopanib (Standard), and synthesized compounds (test inhibitor) were freshly prepared in dimethyl sulfoxide (DMSO) at a single concentration of 10 µM. Master mix (6 µl of 5x Kinase Buffer + 1 µl of 500 µM ATP + 1 µl of PTK Substrate (Poly-Glu, Tyr 4:1) (10 mg/ml) + 17 µl of distilled water) was prepared and 25 µl added to each well. 5 µl of test Inhibitors were added to each well at concentrations 10-fold higher than the desired final concentrations (10 µM) except blank, standard, and positive control. Further, 5 µl of the standard was added to respective wells excluding wells of blank, test inhibitors, and positive control. 5 µl of the diluent solution was added to the blank and positive control wells respectively. 20 µl of 1x Kinase Buffer 1 was added to the blank wells. The reaction was initiated by adding 20 µl of diluted VEGFR2 (KDR) protein kinase (1 ng/µl) to the wells designated as positive control and test inhibitors. The plate was incubated at 30°C for 45 minutes. During the incubation, the Kinase-Glo™ MAX reagent thawed and 50 µl of Kinase-Glo™ MAX reagent was added to each well at the end of the 45-minute reaction. The plate was covered with aluminum foil and incubated at room temperature for 15 minutes. Immediately read on microplate reader capable of reading luminescence. The Blank value was subtracted from all other readings. Results are presented as % VEGFR2 kinase activity inhibition at 10 µM and compared to Pazopanib as a reference VEGFR2 inhibitor. Further compounds which showed more than 50 % VEGFR2 kinase activity inhibition at 10 µM were used further. The inhibition of VEGFR2 (KDR) kinase activity was measured in the presence of increasing inhibitor concentrations. Results are expressed as the % of control (kinase activity in the absence of inhibitor, set at 100%). The IC_{50} values of test inhibitors were calculated by using different concentrations[32–34].

***In-vitro* Anticancer Activity (SRB assay)**

The cytotoxic activity of the compounds was evaluated by colorimetric SRB (Sulforhodamine B) assay. The cancer cell lines such as MCF-7 & MDA-MB-231 (Breast cancer), HEK-293 (Kidney cancer), A549 (lung cancer) were used and Doxorubicin was kept as a positive control. Briefly, logarithmically growing cells were seeded in a 96-well plate (seeding density: MCF-7: 5,000 cells/well, MDA-MB-231 (10,000 cells/well), HEK-293: 7,500 cells/well, and A549: 5,000 cells/well incubated for 24 hr in humidified condition (5% CO_2) at 37°C and then observed under a microscope. Appropriate dilutions of test

compounds were prepared and then added to the wells in triplicate along with DMSO as vehicle control. Then plates were incubated in 5% CO_2 humidified condition at 37°C for 72 hr. At the end of the incubation period, each well was treated with 50 µl of ice-cold trichloroacetic acid (10% TCA) and it was further incubated for 1-2 hr at 4°C for cell fixation. To remove excess TCA, cells were washed with distilled water and allowed to dry in the air. After drying, 50 µl of SRB solution (0.045% w/v) was added to each well and allowed to stain at room temperature for 30 mins. The plate was washed with 1% v/v acetic acid to remove the unbound dye and was allowed to dry in the air. About 100 µl of 10 mM unbuffered tris base (pH 10.5) was added to each well and the plates were gently shaken for 5 mins on a shaker platform to extract the bound SRB. The absorbance was measured using an Epoch microplate reader at a wavelength of 510nm.

A concentration of 25 µM of test compounds was used for initial screening in all cell lines. The ones with >50% inhibition were taken forward for GI_{50} determination (test compound concentration inhibiting 50% of the cell population). To determine the GI_{50} value of test compounds in respective cell lines, a total of nine concentrations (i.e. 0.5, to 100 µM) in triplicate were used. The GI_{50} was then calculated by regression analysis and expressed in µM using a mean of triplicate[35].

Half maximal growth inhibition (GI_{50}) calculation

The molecules exhibited a convincingly potential cytotoxic effect in most of the tested cancer cell lines and were found to be active at less than 50 µM concentration. Compounds indicating 50 % or more growth inhibition in tested cell lines were further screened at nine doses (i.e. 0.5 µM, 0.1, 5, 1, 5, 10, 30, 50, and 100 µM) and growth inhibition was calculated as GI_{50} value reflecting the concentration of drugs required to cause 50 % cell growth inhibition[35–37].

RESULTS AND DISCUSSION

In silico pharmacokinetic screening

In present study we have designed and developed some ethyl 2-(((1H-benzo[d]imidazol-2-yl)methyl)amino)thiazole-4-carboxylate derivatives as potential VGFR inhibitors. In accordance with Lipinski's and Veber's rule (Table 2), the log P values of all the molecules were between the ranges 0.22 to 3.29 which indicates optimum lipophilicity. Lipophilicity is a significant feature of the molecule that affects how it works in the body. It is determined by the compound's Log P value, which measures the drug's permeability in the body to reach the target tissue. The molecular weight of all the molecules was around 500 Da which indicates active better transport of the molecules through biological membrane. Fortunately, the Lipinski rule of 5 had not been compromised by the compounds. All the compounds accepted the Lipinski rule of 5 .The total polar surface area (TPSA) and the number of rotatable bonds have been found to better discriminate between compounds that are orally active or not. According to Veber's rule, TPSA should be ≤ 140 and number of rotatable bonds should be ≤ 10. It was observed that, compounds **AP33, AP40, AP42, AP48 and AP56** violated the Veber's rule, as it has TPSA 162.24, 162.24, 177.11, 158.94 and 142.72 $Å^2$.

In order to further optimize the compounds, pharmacokinetics and drug-likeness properties were calculated for each one. All the compounds showed no penetration to the blood-brain barrier (BBB). The log *Kp* (skin penetration, cm/s) and bioavailability values of all the compounds were within acceptable limits. (Table 3).The GI absorption of all the compounds was found to be high except for **AP33, AP39, AP40, AP41, AP42, AP43, AP46, AP47, AP48, AP50, AP56 and AP60.**

In acute toxicity predictions, it was concluded that, among the 30 screened molecules through ADMET analysis, all the compounds fall in class IV of toxicity [which means harmful if swallowed ($300<LD_{50}\leq2000$)] [13], which means they possess drug-like properties and hence were subjected to molecular docking studies (Table 4).

Table 2. Lipinski rule of 5 and Veber's rule calculated for molecules

Compound Codes	Lipinski rule of five					Veber's rule	
	Log P	Mol. Wt.	HBA	HBD	Violations	Total polar surface area ($Å^2$)	No. of rotatable bonds
NL	4.62	536.58	8	1	0	104.16	8
AP31	2.10	330.36	5	1	0	116.42	7
AP32	3.48	406.46	5	1	0	116.42	8
AP33	2.76	451.46	7	1	0	162.24	9
AP34	4.02	485.35	5	1	0	116.42	8
AP35	3.69	424.45	6	1	0	116.42	8
AP36	3.96	440.90	5	1	0	116.42	8
AP37	3.80	420.48	5	1	0	116.42	8

AP38	3.46	436.48	6	1	0	125.65	9
AP39	3.03	422.46	6	2	0	136.65	6
AP40	2.65	451.46	7	1	0	162.24	9
AP41	3.04	422.46	6	2	0	136.65	8
AP42	2.49	454.46	8	4	0	177.11	8
AP43	3.02	452.48	7	2	0	145.88	9
AP44	3.45	436.48	6	1	0	125.65	9
AP45	3.87	432.49	5	1	0	116.42	9
AP46	4.28	456.52	5	1	0	116.42	8
AP47	1.96	496.45	9	1	0	129.10	10
AP48	3.16	484.55	7	1	0	158.94	9
AP49	3.45	449.53	5	1	0	119.66	9
AP50	4.47	474.46	8	1	0	116.42	9
AP51	2.30	344.29	5	1	0	116.42	7
AP52	2.71	358.41	5	1	0	116.42	8
AP53	3.06	372.44	5	1	0	101.42	9
AP54	3.86	475.56	5	1	0	119.66	10
AP55	2.76	370.43	5	1	0	116.42	8
AP56	2.28	402.42	7	1	0	142.72	10
AP57	3.72	412.51	5	1	0	116.42	8
AP58	4.39	448.54	5	1	0	116.42	8
AP59	4.13	434.51	5	1	0	116.42	8
AP60	5.19	506.57	5	1	1	116.42	8

Where: Mol. Wt., molecular weight; HBA, hydrogen bond acceptors; HBD, hydrogen bond donors

Table 3. The pharmacokinetics and drug-likeness properties of developed compounds

Compound codes	Pharmacokinetics									Drug-likeness			
	GI abs.	BBB pen.	P-gp sub.	CYP1A2 inhibitors	CYP2C19 inhibitors	CYP2C9 inhibitors	CYP2D6 inhibitors	CYP3A4 inhibitors	$LogK_p$ (skin permeation, cm/s)	Ghose	Egan	Muegge	Bioavailability Score
NL	H	N	Y	N	Y	Y	Y	Y	-6.46	N	Y	Y	0.55
AP31	H	N	N	N	Y	Y	N	N	-6.68	Y	Y	Y	0.55
AP32	H	N	N	N	Y	Y	N	Y	-5.97	Y	Y	Y	0.55
AP33	L	N	N	N	Y	Y	N	Y	-6.37	Y	N	N	0.55
AP34	H	N	N	N	Y	Y	N	Y	-5.97	N	Y	Y	0.55
AP35	H	N	N	N	Y	Y	N	Y	-6.01	Y	Y	Y	0.55
AP36	H	N	N	N	Y	Y	N	Y	-5.74	Y	Y	Y	0.55
AP37	H	N	N	N	Y	Y	N	Y	-5.80	Y	Y	Y	0.55
AP38	H	N	N	N	Y	Y	N	Y	-6.18	Y	Y	Y	0.55
AP39	L	N	N	N	Y	Y	N	Y	-6.32	Y	N	Y	0.55
AP40	L	N	N	N	Y	Y	N	Y	-6.37	Y	N	N	0.55
AP41	L	N	N	N	Y	Y	N	Y	-6.32	Y	N	Y	0.55
AP42	L	N	N	N	N	Y	N	Y	-6.63	Y	N	N	0.55
AP43	L	N	N	N	Y	Y	N	Y	-6.53	Y	N	Y	0.55
AP44	H	N	N	N	Y	Y	N	Y	-6.18	Y	Y	Y	0.55
AP45	H	N	N	N	Y	Y	N	Y	-5.83	Y	Y	Y	0.55
AP46	L	N	N	N	Y	Y	N	Y	-5.39	Y	Y	N	0.55
AP47	L	N	N	N	Y	Y	N	Y	-6.77	N	N	N	0.55
AP48	L	N	N	N	Y	Y	N	Y	-6.99	N	N	N	0.55
AP49	H	N	N	N	Y	Y	N	Y	-6.15	Y	Y	Y	0.55
AP50	L	N	N	Y	Y	Y	N	Y	-5.67	N	N	Y	0.55
AP51	H	N	N	N	Y	Y	N	N	-6.77	Y	Y	Y	0.55
AP52	H	N	N	Y	Y	Y	N	Y	-6.53	Y	Y	Y	0.55
AP53	H	N	N	Y	Y	Y	N	Y	-6.36	Y	Y	Y	0.55
AP54	H	N	N	N	Y	Y	N	Y	-6.01	N	Y	Y	0.55
AP55	H	N	N	Y	Y	Y	Y	Y	-6.61	Y	Y	Y	0.55

AP56	L	N	N	N	Y	Y	N	Y	-6.66	Y	N	Y	0.55
AP57	H	N	N	N	Y	Y	Y	Y	-5.71	Y	Y	Y	0.55
AP58	H	N	N	N	Y	Y	N	Y	-5.45	Y	Y	N	0.55
AP59	H	N	N	N	Y	Y	N	Y	-5.63	Y	Y	Y	0.55
AP60	L	N	N	N	Y	Y	N	Y	-4.81	N	N	N	0.55

Where: NL, Native ligand; GI abs., gastrointestinal absorption; BBB pen., blood brain barrier penetration; P-gp sub., p-glycoprotein substrate

Table 4. The predicted acute toxicity of molecules

Compound codes	Parameters							
	LD_{50} (mg/kg)	Toxicity class	Prediction accuracy (%)	Hepatotoxicity	Carcinogenicity	Immunotoxicity	Mutagenicity	Cytotoxicity
				(Probability)				
NL	800	4	23	I (0.55)	I (0.53)	A (0.95)	I (0.54)	I (0.63)
AP31	1000	4	67.38	I (0.63)	I (0.58)	I (0.80)	I (0.57)	I (0.66)
AP32	1000	4	67.38	I (0.63)	I (0.58)	I (0.83)	I (0.56)	I (0.66)
AP33	1000	4	67.38	I (0.57)	A (0.67)	A (0.55)	A (0.87)	I (0.69)
AP34	1000	4	67.38	I (0.59)	I (0.59)	A (0.56)	I (0.61)	I (0.60)
AP35	1000	4	67.38	I (0.59)	I (0.59)	A (0.60)	I (0.61)	I (0.65)
AP36	1000	4	67.38	I (0.59)	I (0.59)	I (0.54)	I (0.60)	I (0.64)
AP37	1000	4	67.38	I (0.65)	I (0.61)	I (0.90)	I (0.55)	I (0.65)
AP38	1000	4	67.38	I (0.64)	I (0.61)	A (0.67)	I (0.52)	I (0.56)
AP39	1000	4	67.38	I (0.63)	I (0.61)	I (0.69)	I (0.58)	I (0.59)
AP40	1000	4	67.38	I (0.57)	A (0.67)	A (0.66)	I (0.87)	I (0.69)
AP41	1000	4	67.38	I (0.63)	I (0.61)	A (0.75)	I (0.58)	I (0.59)
AP42	1000	4	67.38	I (0.62)	I (0.64)	A (0.59)	I (0.59)	I (0.55)
AP43	1000	4	67.38	I (0.65)	I (0.63)	A (0.93)	I (0.55)	I (0.52)
AP44	1000	4	67.38	I (0.64)	I (0.60)	A (0.50)	I (0.55)	I (0.52)
AP45	1000	4	67.38	I (0.63)	I (0.58)	I (0.53)	I (0.57)	I (0.65)
AP46	1000	4	67.38	I (0.63)	I (0.58)	A (0.52)	I (0.56)	I (0.66)
AP47	1000	4	54.26	I (0.59)	A (0.62)	A (0.83)	A (0.85)	I (0.65)
AP48	1000	4	51.05	I (0.55)	I (0.66)	A (0.55)	I (0.69)	I (0.61)
AP49	1000	4	67.38	I (0.63)	I (0.64)	A (0.58)	I (0.55)	I (0.61)
AP50	1000	4	67.38	I (0.61)	I (0.59)	I (0.57)	I (0.58)	I (0.64)
AP51	1000	4	67.38	I (0.67)	I (0.62)	I (0.97)	I (0.58)	I (0.65)
AP52	1000	4	67.38	I (0.68)	I (0.62)	I (0.95)	I (0.61)	I (0.67)
AP53	1000	4	67.38	I (0.72)	I (0.60)	I (0.91)	I (0.64)	I (0.68)
AP54	1000	4	54.26	I (0.62)	I (0.63)	A (0.87)	I (0.57)	I (0.61)
AP55	1000	4	67.38	I (0.65)	I (0.59)	I (0.78)	I (0.54)	I (0.68)
AP56	1000	4	67.38	I (0.66)	I (0.60)	I (0.96)	I (0.58)	I (0.64)
AP57	1000	4	67.38	I (0.71)	I (0.59)	I (0.85)	I (0.57)	I (0.69)
AP58	1000	4	67.38	I (0.68)	I (0.63)	I (0.83)	I (0.55)	I (0.58)
AP59	1000	4	67.38	I (0.68)	I (0.63)	I (0.77)	I (0.55)	I (0.58)
AP60	1000	4	67.38	I (0.63)	I (0.58)	I (0.58)	I (0.56)	I (0.66)

Where: I, Inactive; A, Active

Screening of derivatives through molecular docking

The binding affinities of the derivatives have been compared with the binding mode of native ligand present in the crystal structure of VEGFR-2 enzyme (PDB ID: 6XKV). The active amino acid residues, bond length, bond category, bond type, ligand energies, and binding affinities of the most potent derivatives are in detail tabulated in Table 5. The docking poses are depicted in Figure 4.

The compound AP35 exhibited -8.7 kcal/mol of binding affinity and formed four conventional hydrogen bonds and three carbon hydrogen bonds with Glu885, Cys1024, Ile1025 and Asp1046. It also showed some hydrophobic interactions (Pi-Sigma, Pi-Alkyl) with Ile888, Leu889 and Ala881. The compound AP37 exhibited -8.7 kcal/mol of binding affinity and formed four conventional hydrogen bonds and three carbon hydrogen bonds with Glu885, Cys1024, Ile1025 and Asp1046. It also showed some hydrophobic interactions (Pi-Sigma, Alkyl, Pi-Alkyl) with Ile888, Leu889 and Ala881.

The compound AP41 showed -8.8 kcal/mol of binding affinity and formed four conventional hydrogen bonds and three carbon hydrogen bonds with Glu885, Ala881, Cys1024, Ile1025 and Asp1046. It also showed some hydrophobic interactions (Pi-Sigma, Pi-Alkyl) with Ile888, Leu889 and Ala881. The compound AP42 showed -8.9 kcal/mol of binding affinity and formed six conventional hydrogen bonds

with Gly1102, Ala881, Arg1051 and Asp1056. It also showed some hydrophobic interactions (Pi-Alkyl) withLys1055, Arg1032 and electrostatic interactions (Pi-Anion) with Asp1056 and Asp1058.
The compound AP47 showed -9.1 kcal/mol of binding affinity and formed seven conventional hydrogen bonds with Leu840, Asp1058, Arg1032, Asn923, Ser925 and Arg1051. It also showed some hydrophobic interactions (Pi-Alkyl) with Pro839, Arg842 and Arg1032. The compound AP48 showed -9 kcal/mol of binding affinity and formed five conventional hydrogen bonds with Asp1046, Lys868, Arg1027, Leu1049 and one Carbon hydrogen bond with Gly1048. It also showed some hydrophobic interactions (Pi-Pi T-shaped, Alkyl, Pi-Alkyl) with His1026, Ala881, Leu1049, Arg1027, and electrostatic interactions (Pi-Anion) Glu885, Asp1046. The compound AP50 showed -8.9 kcal/mol of binding affinity and formed seven conventional hydrogen bonds with Asp1046, Lys868, Arg1027, Leu1049 and one carbon hydrogen bond with Gly1048. It also showed some hydrophobic interactions (Alkyl, Pi-Alkyl) with Ala881, Leu1049, Arg1027, Ile888, Leu1019, Cys1024, and electrostatic interactions (Pi-Anion) with Glu885.
The compound AP51 showed -8.8 kcal/mol of binding affinity and formed four conventional hydrogen bonds with Lys868, Arg1027, Leu1049 and one carbon hydrogen bond with His1026. It also showed some hydrophobic interactions (Pi-Alkyl) with Arg1027 and electrostatic interactions (Pi-Anion) with Glu885, Asp1028, and Asp1046. The compound AP55 showed -8.9 kcal/mol of binding affinity and formed four conventional hydrogen bonds with Lys868, Arg1027, Leu1049 and one carbon hydrogen bond with His1026. It also showed some electrostatic interactions (Pi-Anion) with Asp1028, Asp1046. The compound AP58 showed -9 kcal/mol of binding affinity and formed four conventional hydrogen bonds with Glu885, Cys1024, Ile1025 and one carbon hydrogen bond with Glu885, Ile1025. It also showed some hydrophobic interactions (Pi-Sigma, Pi-Alkyl) with Leu889, Val898, Leu889, Ile888, and Ala881. Out of the 30 screened derivatives, **AP35, AP37, AP41, AP42, AP47, AP48, AP50, AP51, AP55,** and **AP58** exhibited binding affinity greater than native ligand and formed four and more than four hydrogen bonds with enzyme are considered as most potent and hence selected for wet lab synthesis followed by biological evaluation.

Table 5. The active amino residues, bond length, bond category, bond type, ligand energies, and docking scores

Active Amino acid	Bond length	Bond Type	Bond Category	Ligand Energy	Docking score
AP35					
GLU885	2.61482	Hydrogen Bond	Conventional Hydrogen Bond	929.35	-8.7
	2.37758				
CYS1024	2.73732				
ILE1025	2.46504				
GLU885	2.85922		Carbon Hydrogen Bond		
ASP1046	3.41824				
ILE1025	3.16985				
ILE888	3.78589	Hydrophobic	Pi-Sigma		
LEU889	3.74502				
LEU889	4.99634		Pi-Alkyl		
ALA881	4.79262				
AP37					
GLU885	2.60207	Hydrogen Bond	Conventional Hydrogen Bond	928.83	-8.7
	2.41676				
CYS1024	2.78553				
ILE1025	2.34923				
GLU885	2.88147		Carbon Hydrogen Bond		
ASP1046	3.46027				
ILE1025	3.21713				
ILE888	3.75549	Hydrophobic	Pi-Sigma		

LEU889	3.89984				
ALA881	4.15081		Alkyl		
LEU889	5.06642		Pi-Alkyl		
ALA881	4.76597				
AP41					
GLU885	2.28696	Hydrogen Bond	Conventional Hydrogen Bond	929.15	-8.8
ALA881	2.51187				
CYS1024	2.73747				
ILE1025	2.4988				
GLU885	2.90277		Carbon Hydrogen Bond		
ASP1046	3.30094				
ILE1025	3.21427				
ILE888	3.85261	Hydrophobic	Pi-Sigma		
LEU889:	3.69903				
LEU889	5.03892		Pi-Alkyl		
ALA881	4.89391				
AP42					
ASP1056	2.51394	Hydrogen Bond	Conventional Hydrogen Bond	959.91	-8.9
	2.70806				
ASP1056	2.66281				
GLY1102	2.33835				
ARG1051	1.87039				
ARG1051	2.64242				
ASP1056	4.78197	Electrostatic	Pi-Anion		
ASP1058	4.98601				
LYS1055	4.9248	Hydrophobic	Pi-Alkyl		
ARG1032	5.11637				
AP47					
LEU840	2.5405	Hydrogen Bond	Conventional Hydrogen Bond	1094.37	-9.1
	2.79287				
ASP1058	2.13806				
ARG1032	2.29341				
ASN923	2.70085				
SER925	2.71798				
ARG1051	1.89065				
PRO839	5.31223	Hydrophobic	Pi-Alkyl		
ARG842	4.88384				
ARG1032	5.21409				
AP48					
ASP1046	2.3222	Hydrogen Bond	Conventional Hydrogen Bond	1162.06	-9
LYS868	1.91745				
ARG1027	2.12435				
ARG1027	2.13972				
LEU1049	2.60684				
GLY1048	3.16094		Carbon Hydrogen Bond		
GLU885	4.71955	Electrostatic	Pi-Anion		
ASP1046	4.00467				
HIS1026	5.18136	Hydrophobic	Pi-Pi T-shaped		
ALA881	4.31512		Alkyl		
LEU1049	3.9466				

ARG1027	3.9804		Pi-Alkyl		
ARG1027	4.3224				
AP50					
ASP1046	2.25177	Hydrogen Bond	Conventional Hydrogen Bond	826.9	-8.9
	2.52659				
ILE1025	2.34685				
LYS868	2.03457				
ARG1027	1.76464				
ARG1027	2.32363				
LEU1049	2.63547				
GLY1048	3.27997		Carbon Hydrogen Bond		
ASP1028	3.5821	Halogen	Halogen (Fluorine)		
GLU885	4.75529	Electrostatic	Pi-Anion		
ALA881	4.46122	Hydrophobic	Alkyl		
LEU1049	3.9317				
ARG1027	4.93882				
ILE888	5.31991		Pi-Alkyl		
LEU1019	5.07932				
CYS1024	5.28047				
ARG1027	4.09261				
AP51					
LYS868	2.3188	Hydrogen Bond	Conventional Hydrogen Bond	716.18	-8.8
ARG1027	1.85709				
ARG1027	2.53765				
LEU1049	2.25942				
HIS1026	3.5315		Carbon Hydrogen Bond		
GLU885	4.52804	Electrostatic	Pi-Anion		
ASP1028	3.66111				
ASP1046	4.59172				
:ASP1046	3.64156				
ARG1027	5.49242	Hydrophobic	Pi-Alkyl		
AP55					
LYS868	2.34644	Hydrogen Bond	Conventional Hydrogen Bond	1760.72	-8.9
ARG1027	1.84879				
ARG1027	2.73237				
LEU1049	2.21548				
HIS1026	3.49891		Carbon Hydrogen Bond		
GLU885	4.57606	Electrostatic	Pi-Anion		
ASP1028	3.74298				
ASP1046	4.57077				
ASP1046	3.6344				
AP58					
GLU885	2.60269	Hydrogen	Conventional Hydrogen	941.09	-9

	2.56686	Bond	Bond		
CYS1024	2.78028				
ILE1025	2.42394				
GLU885	2.81667		Carbon Hydrogen Bond		
ILE1025	3.38527				
LEU889	3.71882	Hydrophobic	Pi-Sigma		
VAL898	5.4416		Pi-Alkyl		
LEU889	4.97264				
ILE888	4.32249				
ALA881	5.05309				
NL					
CYS919	2.73884	Hydrogen Bond	Conventional Hydrogen Bond	933.34	-8.7
	3.06352				
LEU840	3.95706	Hydrophobic	Pi-Sigma		
HIS1026	5.40986		Pi-Pi T-shaped		
ILE888	4.13805		Alkyl		
CYS1024	3.8825				
LEU889	5.27859				
VAL848	5.45953		Pi-Alkyl		
ALA866	3.95797				
CYS919	5.0877				
LEU1035	4.42133				
CYS1024	5.44712				
HIS1026	5.28315				

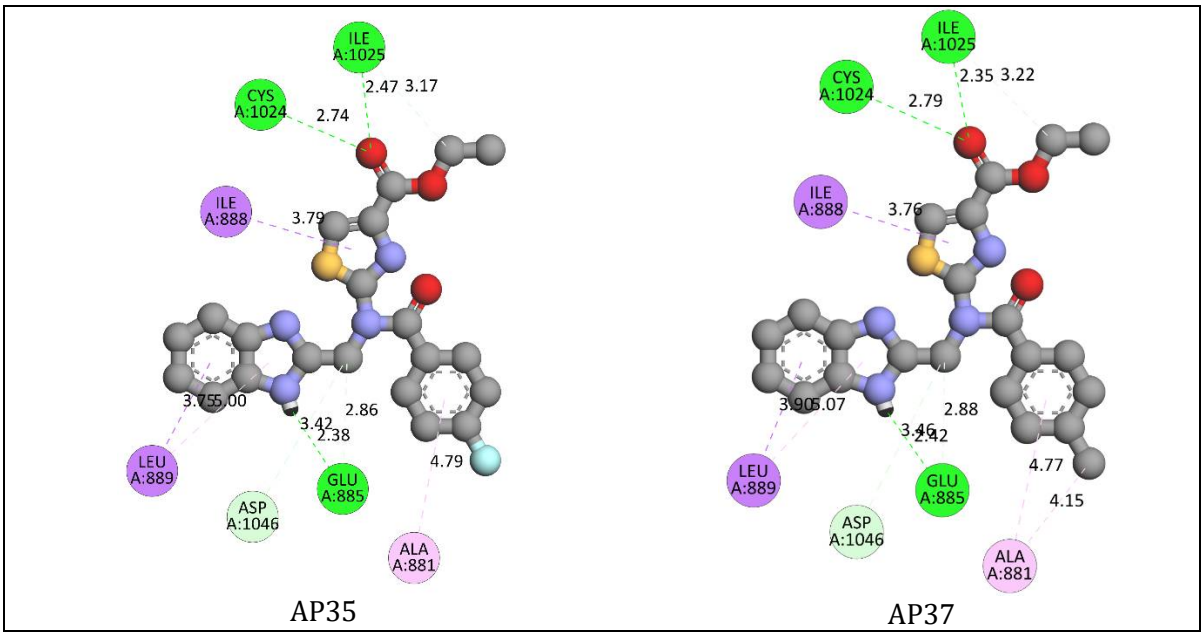

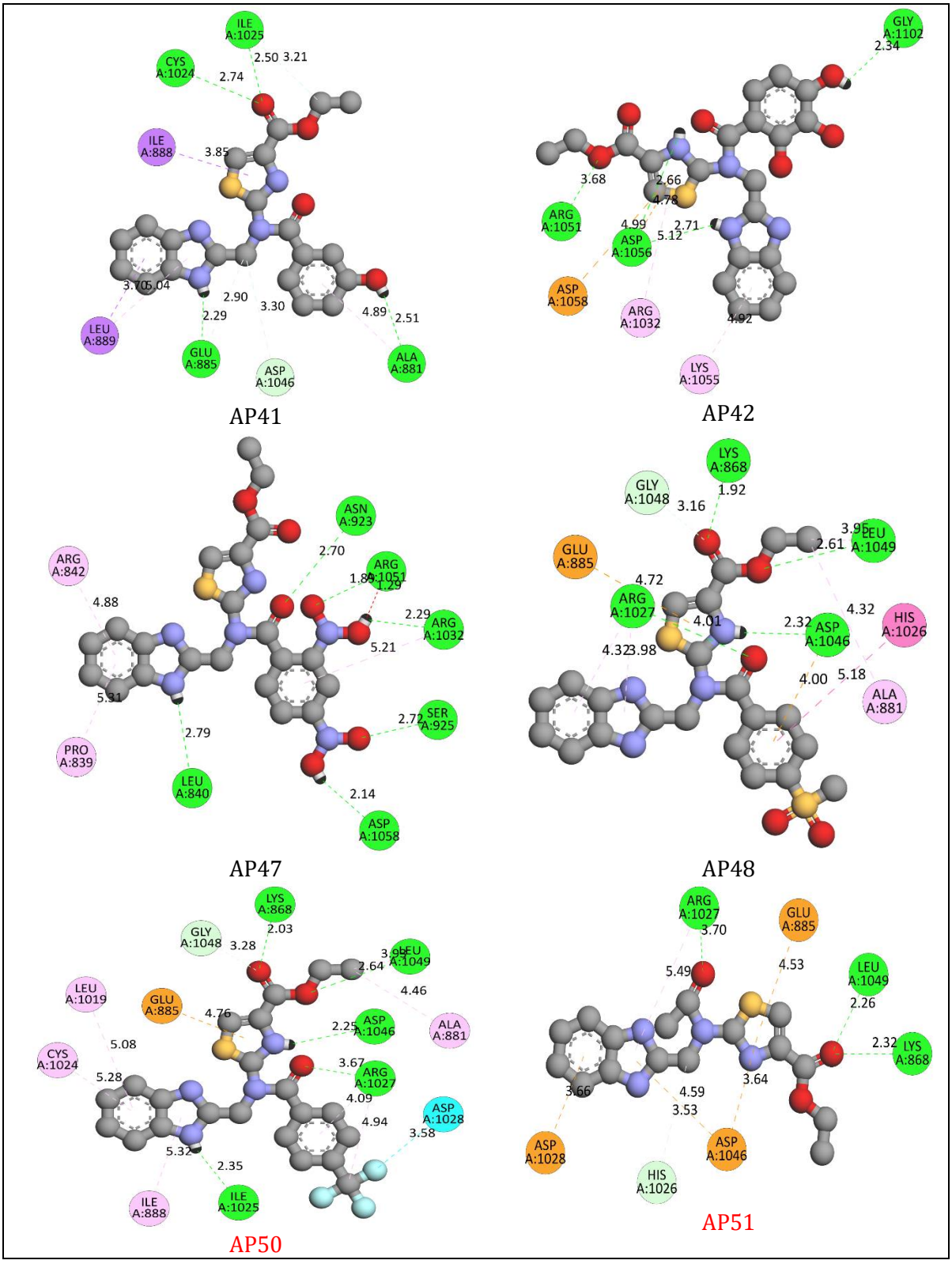
ILE A:1025
CYS A:1024
ILE A:888
LEU A:889
GLU A:885
ASP A:1046
ALA A:881
AP41
GLY A:1102
ARG A:1051
ASP A:1056
ASP A:1058
ARG A:1032
LYS A:1055
AP42
ASN A:923
ARG A:842
ARG A:1051
ARG A:1032
SER A:925
PRO A:839
LEU A:840
ASP A:1058
AP47
LYS A:868
GLY A:1048
LEU A:1049
GLU A:885
ARG A:1027
ASP A:1046
HIS A:1026
ALA A:881
AP48
LYS A:868
GLY A:1048
LEU A:1049
LEU A:1019
GLU A:885
ASP A:1046
ALA A:881
CYS A:1024
ARG A:1027
ASP A:1028
ILE A:888
ILE A:1025
AP50
ARG A:1027
GLU A:885
LEU A:1049
LYS A:868
ASP A:1028
ASP A:1046
HIS A:1026
AP51

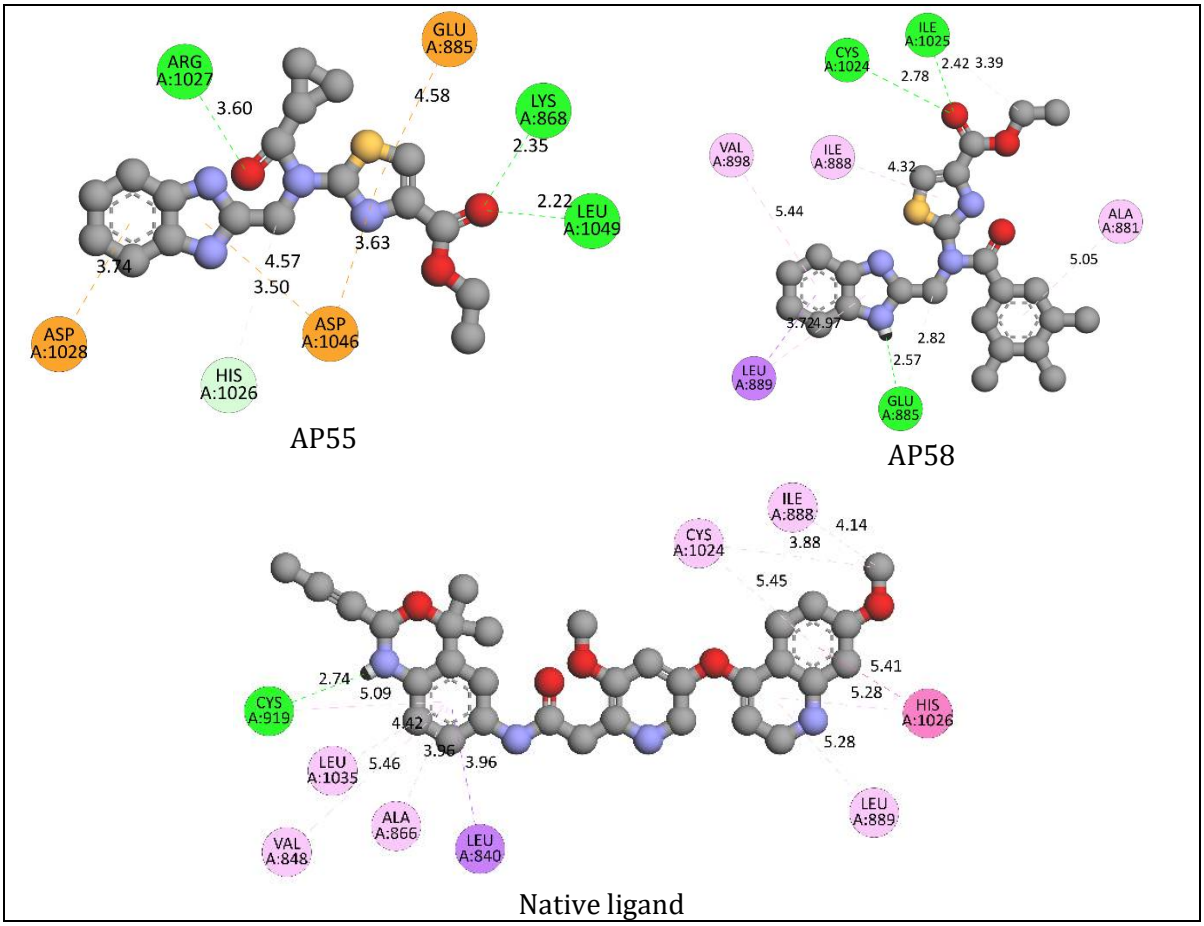

Figure 4. The docking poses of native ligand and most potent derivatives

Biological Evaluation

VEGFR2 (KDR kinase inhibitory activity assay)

All the synthesized compounds were screened to evaluate their ability to inhibit VEGFR2 kinase activity using Pazopanib as a reference compound. The VEGFR2 kinase inhibition assay was performed at a testing dose of 10 µM (Figure 5). The VEGFR2 inhibitory activity of these compounds was analyzed and compared with the reference VEGFR2 inhibitor (Table 6).

Table 6. The % VEGFR2 kinase inhibition at 10 µM

Comp. Code	% VEGFR2 kinase Inhibition at 10 µM
AP35	41.04 ± 1.28
AP37	24.04 ± 1.37
AP41	33.11 ± 2.65
AP42	27.64 ± 0.91
AP47	87.72 ± 1.32
AP48	74.27 ± 0.89
AP50	63.11 ± 0.99
AP51	47.72 ± 2.16
AP55	37.61 ± 1.12
AP58	44.51 ± 1.26
Pazopanib	100 ± 1.05

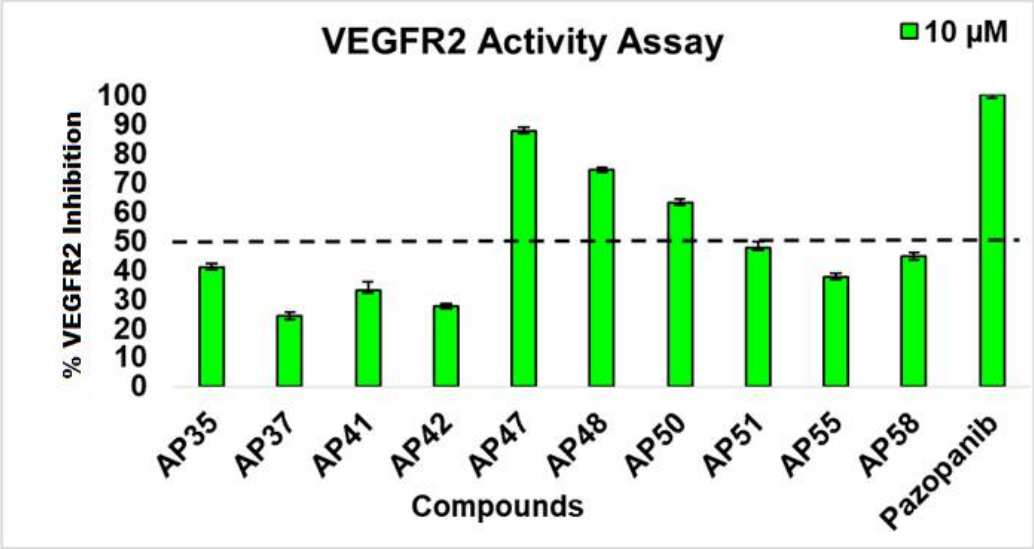

Figure 4. Screening of compounds against VEGFR2 kinase activity at 10 µM

Amongst the tested compounds, three compounds (**AP47, AP48, and AP50**) inhibited VEGFR2 kinase by more than 50%. Compounds **AP47, AP48, and AP50** were found to be the most active VEGFR2 inhibitor that exhibited 87.72, 74.72, and 63.11% inhibition respectively at 10 µM. They were selected and subjected to IC_{50} value determination (Table 7). Compounds **AP47** and **AP50** showed excellent VEGFR2 kinase inhibitory activity at IC_{50} 2.77 and 4.90 µM respectively whereas pazopanib displayed VEGFR2 kinase inhibitory activity at 0.092 µM. Compound **AP47** was found to be the most potent VEGFR2 inhibitor.

Table 7. IC_{50} values of compounds as VEGFR2 kinase inhibitors

Sr. No.	Comp. Code	Enzyme kinase Inhibition IC_{50} (µM)
1	AP47	2.77 ± 0.48
2	AP48	4.90 ± 0.13
3	AP50	6.13 ± 0.65
4	Pazopanib	0.092 ± 0.43

***In-vitro* Anticancer Activity (SRB assay)**

Compound Screening

The cytotoxicity of synthesized compounds was evaluated against five cancerous cell lines breast (MCF-7 & MDA-MB-231), kidney (HEK-293), and lung (A549) via SRB assay. Initially, synthesized compounds were evaluated for biological screening using SRB assay at a single dose of each compound (25 µM). Doxorubicin (DOX) was used as a positive control. The results obtained from biological screening data are presented in Table 8 and Figure 5.

Among them, it has been noticed that compounds (**AP41**, **AP47**, **AP48**, **AP50**, **AP55** and **AP58**) showed % cell viability less than 50% against A-549, MCF-7 and HEK-293. All the tested compounds (except **AP47**) showed <50% inhibition against MDA-MB-231 at 25 µM concentration. Compounds that displayed >50% inhibition at 25 µM concentration were further taken up for GI_{50} determination (Table 9).

Table 1. % Cell viability obtained from biological screening at 25 µM

Comp. code	**% Viability at 25 µM**			
	MCF-7	**HEK-293**	**A-549**	**MDA-MB-231**
AP35	74.8042	65.2389	64.5269	78.4069
AP37	68.6945	68.4697	68.6378	72.2756
AP41	50.0291	49.7678	50.0064	62.8754
AP42	67.6248	61.2658	62.4682	57.8523
AP47	37.1365	37.5987	32.6217	48.0069
AP48	44.2236	41.3789	39.9657	64.1662
AP50	45.2789	45.1246	42.4324	67.8962
AP51	55.0123	73.6892	68.7324	71.7894
AP55	47.2984	47.7429	46.2984	65.5746
AP58	49.1786	48.9634	48.6547	56.7846
DOX	1.314	2.325	3.3126	2.395

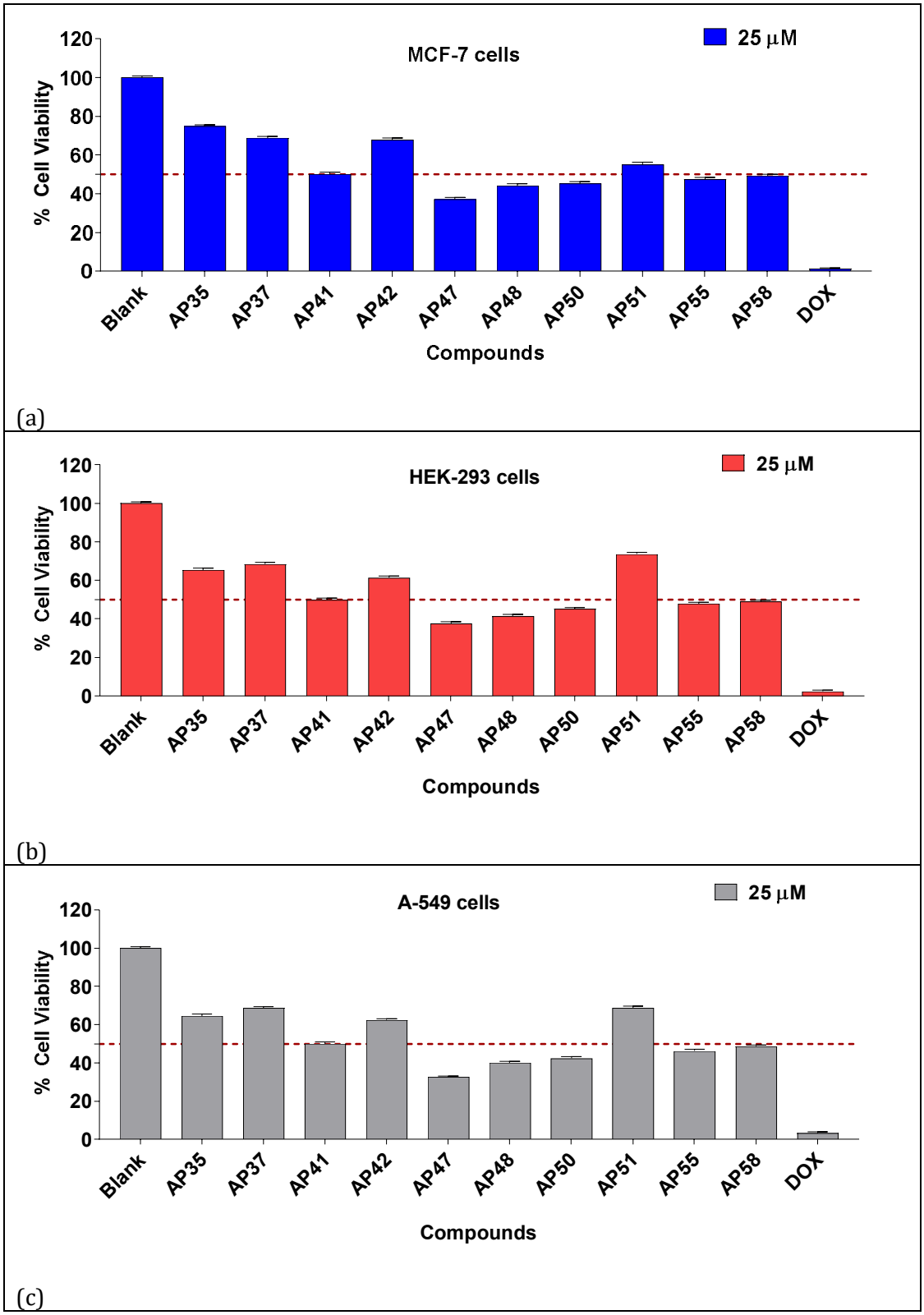
MCF-7 cells
25 µM
% Cell Viability
120
100
80
60
40
20
0
Blank
AP35
AP37
AP41
AP42
AP47
AP48
AP50
AP51
AP55
AP58
DOX
Compounds
(a)
HEK-293 cells
25 µM
% Cell Viability
Compounds
(b)
A-549 cells
25 µM
% Cell Viability
Compounds
(c)

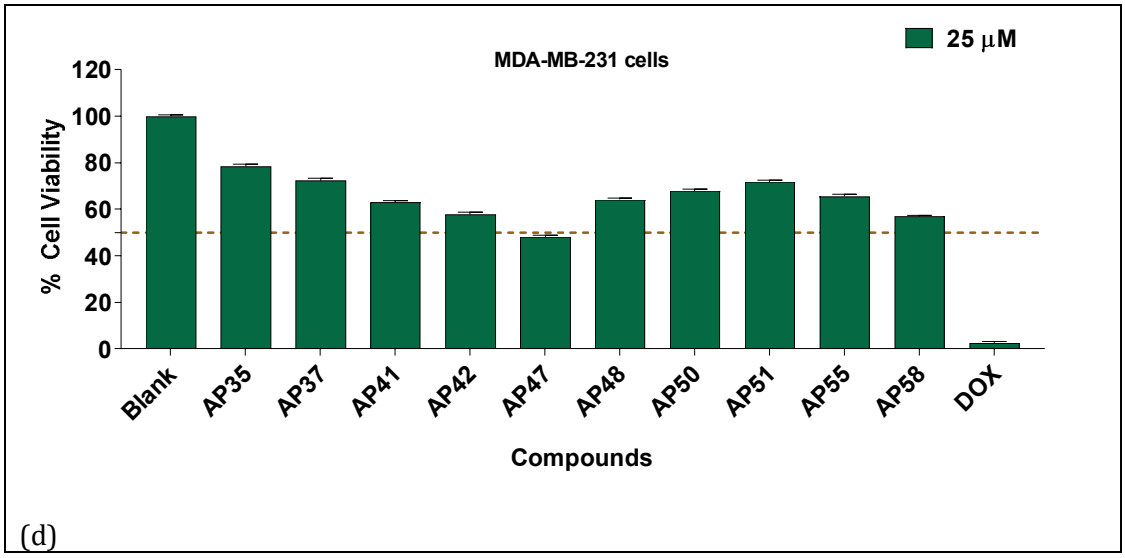

Figure 5. Screening of compounds against a) MCF-7, b) HEK-293, c) A-549 d) MDA-MB-231 cells at 25 µM

Table 9. GI_{50} values of screened compounds against various cell lines

Comp. code	GI_{50} ± SD (µM)			
	MCF-7	HEK-293	A-549	MDA-MB-231
AP41	21.25 ± 0.904	20.29 ± 1.036	17.08 ± 1.121	-
AP47	9.36 ± 1.173	8.24 ± 1.301	6.13 ± 1.198	23.65 ± 0.749
AP48	13.12 ± 1.089	11.89 ± 1.076	8.07 ± 1.721	-
AP50	16.55 ± 1.006	13.23 ± 1.043	11.25 ± 1.135	-
AP55	19.08 ± 1.015	15.36 ± 1.176	12.54 ± 1.074	-
AP58	20.13 ± 1.307	17.31 ± 1.164	14.47 ± 1.486	-
DOX	1.28 ± 1.193	4.89 ± 0.849	1.12 ± 0.687	2.25 ± 1.082

Among the tested compounds, it has been noticed that compound **AP47** was found to be the most potent compound against A-549, HEK-293, and MCF-7 with GI_{50} values of 6.13, 8.24, and 9.36 µM, respectively. Only this compound showed moderate cytotoxicity against MDA-MB-231(GI_{50} =23.65 µM). Compound **AP48** showed good anti-cancer activity against A-549 at GI_{50} values of 8.07 µM, respectively. Compounds (**AP41**, **AP50**, **AP55**, and **AP58**) showed moderate potency against A-549, MCF-7 and HEK-293 (<25 µM). Concentration response curved of the most active compound (AP47) are shown in Figure 6.

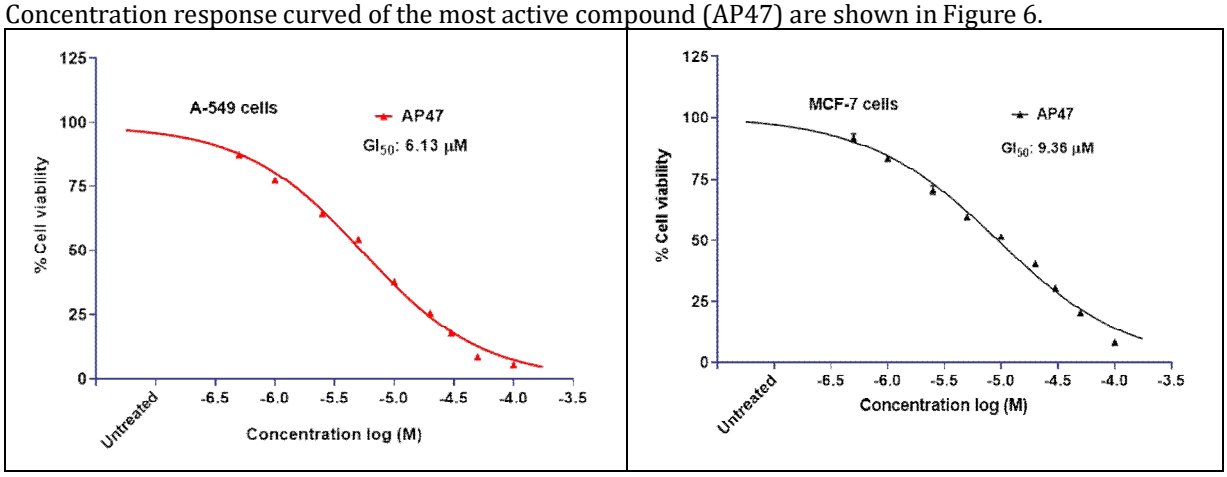

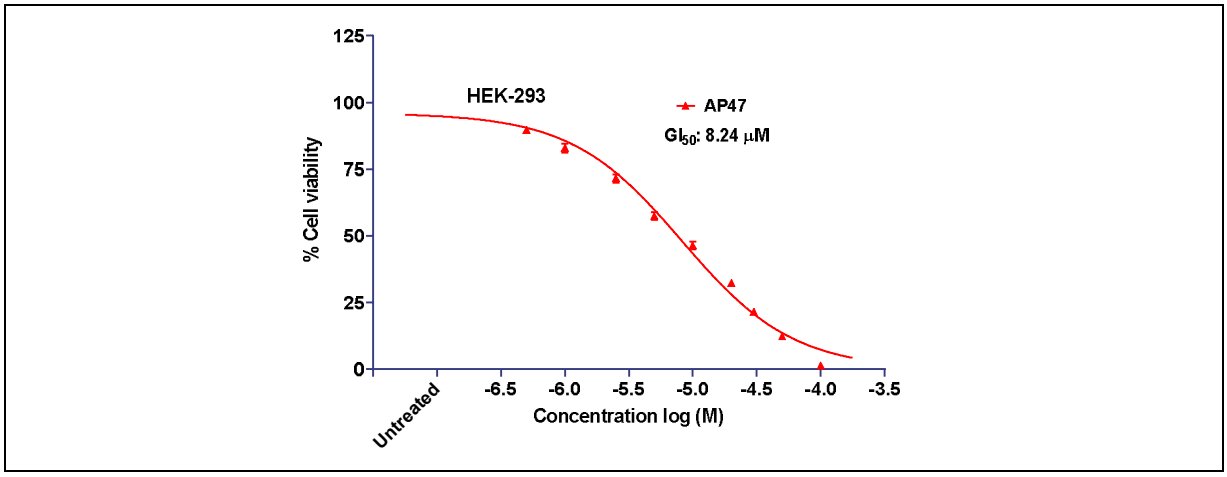

Figure 6. The concentration response curved of the most active compound (AP17)

Structure-activity relationship (SAR)

SAR studies of the synthesized benzo-imidazole compounds revealed the anti-cancer activity dependent on the type of substitutions present on the cyclohexadiene ring attached to the benzo-imidazole ring. The presence of thiazole-4-carboxylate linked through methyl amino to benzo-imidazole ring showed improved activity against A-549, HEK-293, and MCF-7 cancer cell lines. Among the tested compounds, most of the compounds were found to be active against A-549 (lung), MCF-7 (breast), and HEK-293 (kidney) cancer cell lines. All the tested compounds exhibited poor anti-proliferative activities (> 25 µM) against MDA-MB-231 (except compound **AP47**). The compound **AP47** was found to be most cytotoxic (IC_{50} < 10 µM) against MCF-7, HEK-293, and A-549 cell lines except MDA-MB-231. This potent compound **AP47** possesses a 2, 4-dinitro substituted cyclohexadiene ring exhibited potential cytotoxic activity (IC_{50} = 6.13 µM) against the A-549 cell line among the series. This compound also showed good activity against HEK-293 and MCF-7 IC_{50} values of 8.24 µM and 9.36 µM, respectively.

The presence of electron withdrawing groups such as (-NO_2, -CF_3) at the 4th position enhances the anti-cancer activity whereas the presence of electron donating group (–CH_3) at the 4th position on the cyclohexadiene ring decreases the activity. Interestingly, the compound (**AP58)** bearing 2, 6 di-methyl substituted cyclohexadiene exhibited superior cytotoxicity than the mono-substituted compound (**AP37**). The presence of (–CH_3) at the 2nd and 4th position of the cyclohexadiene ring enhances the cytotoxicity. The replacement of this ring with a cyclopropylidene ring decreases the activity against cancer cell lines. However, the compounds bearing –SO_2CH_3 substitution at the 4th position (**AP48**) showed improved cytotoxicity against A-549 and HEK-293 cells with IC_{50} values of 8.07 and 11.89 µM, respectively. The anti-cancer activity of compound **AP41** showed inferior cytotoxicity against all the tested cell lines due to the presence of the –OH group at the 3rd position on the cyclohexadiene ring. A summary of results from the SAR study is presented in Figure 7.

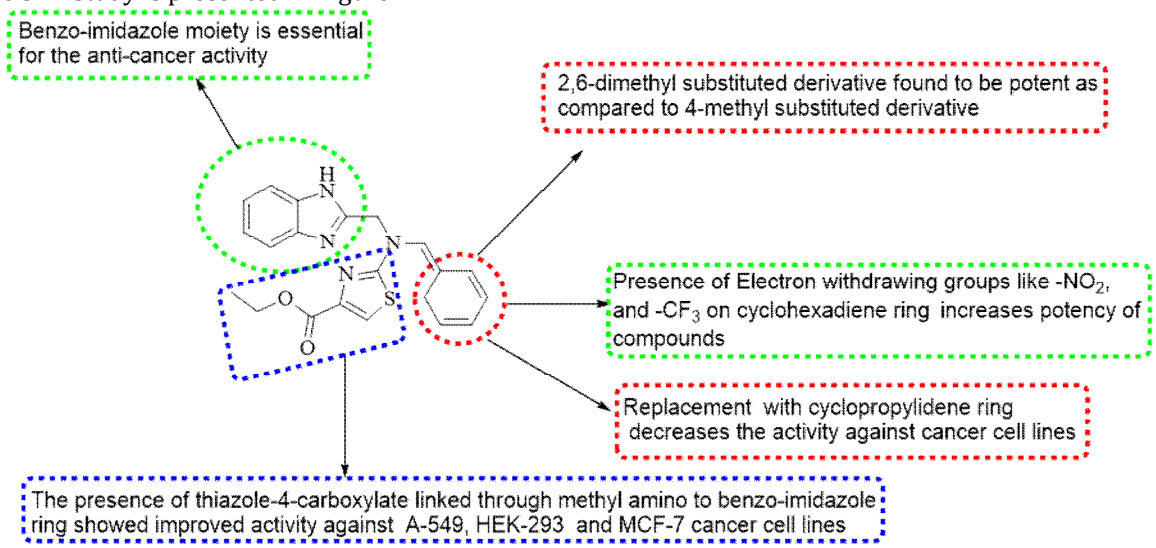

Figure 7. SAR study of benzo-imidazo linked cyclohexa-dienylidene-methylamino thiazole-4-carboxylate as a potent anti-cancer agent.

CONCLUSION

VEGFR-2 is an acronym for Vascular Endothelial Growth Factor Receptor 2, a protein that has a crucial function in the creation of blood vessels, also known as angiogenesis. VEGFR-2 kinase inhibitors are a notable breakthrough in cancer therapy since they specifically target the crucial mechanism of angiogenesis. In conclusion, our comprehensive investigation into the design and development of ethyl 2-(((1*H*-benzo[*d*]imidazol-2-yl)methyl)amino)thiazole-4-carboxylate derivatives as potential VEGFR-2 kinase inhibitors for cancer treatment has yielded promising results. Notably, AP47 emerged as the most potent VEGFR2 inhibitor, displaying excellent kinase inhibitory activity at GI_{50} 2.77 μM. The compound demonstrated significant anti-cancer efficacy across A-549, HEK-293, and MCF-7 cell lines, with the lowest GI_{50} values among the tested compounds. Further, the SAR studies highlighted the influence of substituents on the cyclohexadiene ring attached to the benzo-imidazole ring, with thiazole-4-carboxylate linked through methyl amino showing improved anti-cancer activity. While compound AP47 showcased remarkable potential, other compounds, such as AP48, AP41, AP50, AP55, and AP58, exhibited varying degrees of potency against cancer cell lines. These findings underscore the promise of these compounds as VEGFR2 kinase inhibitors, suggesting a potential avenue for future therapeutic applications in cancer treatment. The results from this study contribute valuable insights into the molecular design of novel agents targeting VEGFR-2, furthering our understanding of potential avenues for the development of effective cancer therapies.

REFERENCES

1. Zhang, Q.; Zheng, P.; Zhu, W. (2020). Research Progress of Small Molecule VEGFR/c-Met Inhibitors as Anticancer Agents (2016-Present). *Molecules*, *25*, doi:10.3390/molecules25112666.
2. Hironaka, S. (2019). Anti-Angiogenic Therapies for Gastric Cancer. *Asia. Pac. J. Clin. Oncol*, *15*, 208–217, doi:10.1111/ajco.13174.
3. Wu, X.; Wang, J.; Liang, Q.; Tong, R.; Huang, J.; Yang, X.; Xu, Y.; Wang, W.; Sun, M.; Shi, J. (2022). Recent Progress on FAK Inhibitors with Dual Targeting Capabilities for Cancer Treatment. *Biomed. Pharmacother. 151*, doi:10.1016/j.biopha.2022.113116.
4. Shibuya, M. (2013). Vascular Endothelial Growth Factor and Its Receptor System: Physiological Functions in Angiogenesis and Pathological Roles in Various Diseases. *J. Biochem. 153*, 13–19, doi:10.1093/jb/mvs136.
5. Yousef, R.G.; Ibrahim, A.; Khalifa, M.M.; Eldehna, W.M.; Gobaara, I.M.M.; Mehany, A.B.M.; Elkaeed, E.B.; Alsfouk, A.A.; Metwaly, A.M.; Eissa, I.H. (2022). Discovery of New Nicotinamides as Apoptotic VEGFR-2 Inhibitors: Virtual Screening, Synthesis, Anti-Proliferative, Immunomodulatory, ADMET, Toxicity, and Molecular Dynamic Simulation Studies. *J. Enzyme Inhib. Med. Chem. 37*, 1389–1403, doi:10.1080/14756366.2022.2070744.
6. Shibuya, M. (2011). Vascular Endothelial Growth Factor (VEGF) and Its Receptor (VEGFR) Signaling in Angiogenesis: A Crucial Target for Anti- and Pro-Angiogenic Therapies. *Genes and Cancer* , *2*, 1097–1105, doi:10.1177/1947601911423031.
7. Sun, S.; Zhang, J.; Wang, N.; Kong, X.; Fu, F.; Wang, H.; Yao, J. (2018). Design and Discovery of Quinazoline- and Thiourea-Containing Sorafenib Analogs as EGFR and VEGFR-2 Dual TK Inhibitors. *Molecules*, *23*, doi:10.3390/molecules23010024.
8. Falcon, B.L.; Chintharlapalli, S.; Uhlik, M.T.; Pytowski, B. (2016). Antagonist Antibodies to Vascular Endothelial Growth Factor Receptor 2 (VEGFR-2) as Anti-Angiogenic Agents. *Pharmacol. Ther. 164*, 204–225, doi:10.1016/j.pharmthera.2016.06.001.
9. Oprea, T.I. (2002). Virtual Screening in Lead Discovery: A Viewpoint. *Molecules*, *7*, 51–62, doi:10. 3390/70100051.
10. Quinn, R.J.; Carroll, A.R.; Pham, N.B.; Baron, P.; Palframan, M.E.; Suraweera, L.; Pierens, G.K.; Muresan, S. (2008). Developing a Drug-like Natural Product Library. *J. Nat. Prod. 71*, 464–468, doi:10.1021/np070526y.
11. Barret, R. (2018). Lipinski's Rule of Five. In *Therapeutical Chemistry*; pp. 97–100.
12. Lipinski, C.A. (2016). Rule of Five in 2015 and beyond: Target and Ligand Structural Limitations, Ligand Chemistry Structure and Drug Discovery Project Decisions. *Adv. Drug Deliv. Rev. 101*, 34–41.
13. Banerjee, P.; Eckert, A.O.; Schrey, A.K.; Preissner, R. (2018). ProTox-II: A Webserver for the Prediction of Toxicity of Chemicals. *Nucleic Acids Res. 46*, W257–W263, doi:10.1093/nar/gky318.
14. Panneerselvam, S.; Yesudhas, D.; Durai, P.; Anwar, M.A.; Gosu, V.; Choi, S. (2015). A Combined Molecular Docking/Dynamics Approach to Probe the Binding Mode of Cancer Drugs with Cytochrome P450 3A4. *Molecules 20*, 14915–14935, doi:10.3390/molecules200814915.
15. Pagadala, N.S.; Syed, K.; Tuszynski, J. (2017). Software for Molecular Docking: A Review. *Biophys. Rev. 9*, 91–102, doi:10.1007/s12551-016-0247-1.
16. Diller, D.J.; Merz, K.M.(2001). High Throughput Docking for Library Design and Library Prioritization. *Proteins Struct. Funct. Genet. 43*, 113–124, doi:10.1002/1097-0134(20010501)43:2<113::AID-PROT1023>3.0.CO;2-T.
17. Morris, G.M.; Lim-Wilby, M. (2008). Molecular Docking. *Methods Mol. Biol. 443*, 365–382, doi:10.1007/978-1-59745-177-2_19.
18. Dar, A.M.; Mir, S. (2017). Molecular Docking: Approaches, Types, Applications and Basic Challenges. *J. Anal. Bioanal. Tech. 08*, doi:10.4172/2155-9872.1000356.

19. Dallakyan, S.; Olson, A.J. (2015). Small-Molecule Library Screening by Docking with PyRx. *Methods Mol. Biol. 1263*, 243–250, doi:10.1007/978-1-4939-2269-7_19.
20. Rappé, A.K.; Casewit, C.J.; Colwell, K.S.; Goddard, W.A.; Skiff, W.M. (1992). UFF, a Full Periodic Table Force Field for Molecular Mechanics and Molecular Dynamics Simulations. *J. Am. Chem. Soc. 114*, 10024–10035, doi:10.1021/ja00051a040.
21. San Diego: (2012).Accelrys Software Inc. Discovery Studio Modeling Environment, Release 3.5. *Accelrys Softw. Inc*.
22. Khan, S.L.; Siddiqui, F.A.; Jain, S.P.; Sonwane, G.M. (2020). Discovery of Potential Inhibitors of SARS-CoV-2 (COVID-19) Main Protease (Mpro) from Nigella Sativa (Black Seed) by Molecular Docking Study. *Coronaviruses*, *2*, 384–402, doi:10.2174/2666796701999200921094103.
23. Chaudhari, R.N.; Khan, S.L.; Chaudhary, R.S.; Jain, S.P.; Siddiqui, F.A. (2020). B-Sitosterol: Isolation from Muntingia Calabura Linn Bark Extract, Structural Elucidation And Molecular Docking Studies As Potential Inhibitor of SARS-CoV-2 Mpro (COVID-19). *Asian J. Pharm. Clin. Res*, *13*, 204–209, doi:10.22159 /ajpcr.2020.v13i5.37909.
24. Khan, S.L.; Siddiqui, F.A.; Shaikh, M.S.; Nema, N. V.; Shaikh, A.A. (2021). Discovery of Potential Inhibitors of the Receptor-Binding Domain (RBD) of Pandemic Disease-Causing SARS-CoV-2 Spike Glycoprotein from Triphala through Molecular Docking. *Curr. Chinese Chem.01*, doi:10.2174/2666001601666210322121802.
25. Khan, S.L.; Sonwane, G.M.; Siddiqui, F.A.; Jain, S.P.; Kale, M.A.; Borkar, V.S. (2020). Discovery of Naturally Occurring Flavonoids as Human Cytochrome P450 (CYP3A4) Inhibitors with the Aid of Computational Chemistry. *Indo Glob. J. Pharm. Sci. 10*, 58–69, doi:10.35652/igjps.2020.10409.
26. Siddiqui, F.A.; Khan, S.L.; Marathe, R.P.; Nema, N. V. (2021). Design, Synthesis, and In Silico Studies of Novel N-(2-Aminophenyl)-2,3- Diphenylquinoxaline-6-Sulfonamide Derivatives Targeting Receptor- Binding Domain (RBD) of SARS-CoV-2 Spike Glycoprotein and Their Evaluation as Antimicrobial and Antimalarial Agents. *Lett. Drug Des. Discov. 18*, 915–931, doi:10.2174/1570180818666210427095203.
27. Shntaif, A.H.; Khan, S.; Tapadiya, G.; Chettupalli, A.; Saboo, S.; Shaikh, M.S.; Siddiqui, F.; Amara, R.R. (2021). Rational Drug Design, Synthesis, and Biological Evaluation of Novel N-(2-Arylaminophenyl)-2,3-Diphenylquinoxaline-6-Sulfonamides as Potential Antimalarial, Antifungal, and Antibacterial Agents. *Digit. Chinese Med. 4*, 290–304, doi:10.1016/j.dcmed.2021.12.004.
28. Khan, S.; Kale, M.; Siddiqui, F.; Nema, N. (2021). Novel Pyrimidine-Benzimidazole Hybrids with Antibacterial and Antifungal Properties and Potential Inhibition of SARS-CoV-2 Main Protease and Spike Glycoprotein. *Digit. Chinese Med. 4*, 102–119, doi:10.1016/j.dcmed.2021.06.004.
29. Khattab, M.; Ragab, F.; Galal, S.; El Diwani, H. (2012). Synthesis of 4-(1H-Benzo[d]Imidazol-2-Yl) Aniline Derivatives of Expected Anti-HCV Activity. *Int. J. Res. Pharm. Chem. 2*, 937–946.
30. Murtaza, S.; Akhtar, M.S.; Kanwal, F.; Abbas, A.; Ashiq, S.; Shamim, S. (2017). Synthesis and Biological Evaluation of Schiff Bases of 4-Aminophenazone as an Anti-Inflammatory, Analgesic and Antipyretic Agent. *J. Saudi Chem. Soc. 21*, S359–S372, doi:10.1016/j.jscs.2014.04.003.
31. Kumar, S.; Kumar, P.; Sati, N. Synthesis and Biological Evaluation of Schiff Bases and Azetidinones of 1-Naphthol. *J. Pharm. Bioallied Sci.* **2012**, *4*, 246–249, doi:10.4103/0975-7406.99066.
32. Elkamhawy, A.; Son, S.; Lee, H.Y.; El-Maghrabey, M.H.; Hamd, M.A.E.; Alshammari, S.O.; Abdelhameed, A.A.; Alshammari, Q.A.; Abdeen, A.; Ibrahim, S.F.; et al. Design, Synthesis, Biological Evaluation, and Molecular Dynamics Studies of Novel Lapatinib Derivatives. *Pharmaceuticals* **2023**, *16*, doi:10.3390/ph16010043.
33. Aoki, K.; Obata, T.; Yamazaki, Y.; Mori, Y.; Hirokawa, H.; Koseki, J.I.; Hattori, T.; Niitsu, K.; Takeda, S.; Aburada, M.; et al. Potent Platelet-Derived Growth Factor-β Receptor (PDGF-BR) Inhibitors: Synthesis and Structure-Activity Relationships of 7-[3-(Cyclohexylmethyl)Ureido]-3-{1-Methyl-1H-Pyrrolo[2,3-b]Pyridin-3-Yl} Quinoxalin-2(1H)-One Derivatives. *Chem. Pharm. Bull.* **2007**, *55*, 255–267, doi:10.1248/cpb.55.255.
34. Lee, K.; Nada, H.; Byun, H.J.; Lee, C.H.; Elkamhawy, A. Hit Identification of a Novel Quinazoline Sulfonamide as a Promising Ephb3 Inhibitor: Design, Virtual Combinatorial Library, Synthesis, Biological Evaluation, and Docking Simulation Studies. *Pharmaceuticals* **2021**, *14*, doi:10.3390/ph14121247.
35. Puri, S.; Stefan, K.; Khan, S.L.; Pahnke, J.; Stefan, S.M.; Juvale, K.(2023). Indole Derivatives as New Structural Class of Potent and Antiproliferative Inhibitors of Monocarboxylate Transporter 1 (MCT1; SLC16A1). *J. Med. Chem. 66*, 657–676, doi:10.1021/acs.jmedchem.2c01612.
36. Basu, P.; Maier, C. Phytoestrogens and Breast Cancer: (2018). In Vitro Anticancer Activities of Isoflavones, Lignans, Coumestans, Stilbenes and Their Analogs and Derivatives. *Biomed. Pharmacother. 107*, 1648–1666, doi:10.1016/j.biopha.2018.08.100.
37. Ameta, K.L.; Rathore, N.S.; Kumar, B. (2012). Synthesis and in Vitro Anti-Breast Cancer Activity of Some Novel 1,5-Benzothiazepine Derivatives. *J. Serbian Chem. Soc. 77*, 725–731, doi:10.2298/JSC110715219A.